Available online at www.sciencedirect.com
ScienceDirect
Journal of Geodynamics 45 (2008) 32–48
JOURNAL OF GEODYNAMICS
http://www.elsevier.com/locate/jog

Slab detachment and mantle plume upwelling in subduction zones: An example from the Italian South-Eastern Alps

Patrizia Macera [a,*], Daniela Gasperini [a], Giorgio Ranalli [b], Rezene Mahatsente [c]

[a] *Dipartimento di Scienze della Terra, University of Pisa, Pisa, Italy*
[b] *Department of Earth Sciences, Carleton University, Ottawa K1S 5B6, Canada*
[c] *Institutte of Geosciences, Christian-Albrecht University, Kiel, Germany*

Received 15 July 2006; received in revised form 9 March 2007; accepted 16 March 2007

Abstract

The geochemical properties of the South-Eastern Alps volcanics (SEAV, Eocene age) call for a within-plate origin of the most primitive basalts, in contrast to the widespread calc-alkaline magmatism which developed some million years later northwestwards along the Periadriatic Lineament. The two contrasting magmatic suites that coexist in the Alpine area define binary mixing relationships in the Sr–Nd and Sr–Pb isotopic space, the end members of which being a crustal component (e.g. lower continental crust) and a HIMU-DMM component (e.g. the SEAV). The occurrence of a HIMU (high μ = high $^{238}U/^{204}Pb$) component, which normally traces mantle plumes of deep mantle origin, in a tectonic regime dominated by collision tectonics (the tertiary convergence of European and Adriatic plates) can be explained by slab detachment and ensuing upwelling of mantle material through the lithospheric gap. We combine geochemical data and geophysical modelling to unravel the evolution of the Alpine slab after interaction with plume material and the genesis of the Alpine magmatism. The combination of changes in negative buoyancy caused by continental subduction and softening of a part of the slab caused by slab–plume interaction may act as a regulator for the time of slab breakoff and, consequently, for the variations of magmatism in the overriding lithosphere above a subduction zone. The thermal evolution of a subducting slab is modified by contact with the plume material which decreases significantly the total strength of the slab and favours slab detachment. Interactions between the HIMU component and the shallower depleted mantle can account for the geochemical characteristics of the SEAV. Counterflows of plume material towards the top of the subducting slab may also increase heating and partial melting of the overriding mantle wedge, giving rise to the calc-alkaline suite outcropping in the proximity of the Periadriatic Lineament.

Keywords: Alpine magmatism; HIMU-OIB; Geochemistry; Subduction; Slab breakoff; Slab rheology

1. Introduction

The Alpine chain is the result of the convergence of a subducting lower plate, consisting of the Mesozoic ocean and the European passive continental margin, and the Adriatic continental upper plate (African promontory) that has occurred from Cretaceous time to present. The gradual closure of the ocean ended with the Adria-Europe collision in the Eocene (Dal Piaz and Venturelli, 1983; Dal Piaz et al., 2003; Stampfli et al., 2001).

The Alpine orogeny began in the eastern Austroalpine in Early-Mid Cretaceous, and subsequently involved the entire Alpine Tethys (Dercourt et al., 1986; von Blankenburg and Davies, 1995; Schmid et al., 1997; Dal Piaz et al., 2003). From the Late Cretaceous, the orogeny extended from the western Austroalpine onwards and was related to the subduction of the Piedmont-Ligurian oceanic lithosphere underneath the Adriatic plate which culminated with the European and Adriatic plate collision at Eocene time (Chopin, 1984; von Blankenburg and Davies, 1995; Schmid et al., 1997; Dal Piaz et al., 2003).

At the end of the Eocene, the subducted complex was exhumed and experienced a new metamorphic imprint (Barrovian metamorphism) during late Eocene-early Oligocene (Mesoalpine phase; Frey et al., 1999). At this time, a post-collision calc-alkaline up to shoshonitic magmatism (plutons, volcanics and volcanoclasts) developed in the proximity of the Periadriatic Fault Lineament from the Aosta valley to Austria and Slovenia (Fig. 1; see Dal Piaz et al., 1979; Venturelli et al., 1984; Bellieni et al., 1996; Macera et al., 2003b). Although this

* Corresponding author. Tel.: +39 050 2215792; fax: +39 050 2215800.
E-mail address: macera@dst.unipi.it (P. Macera).

0264-3707/$ – see front matter © 2007 Elsevier Ltd. All rights reserved.
doi:10.1016/j.jog.2007.03.004

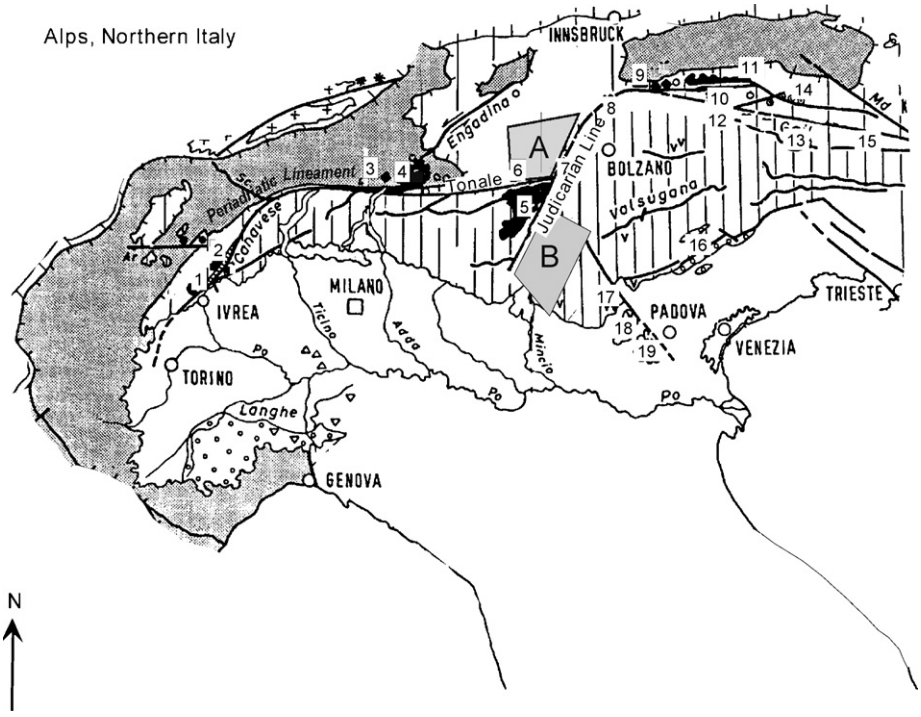

Fig. 1. Sketch map of the Alpine chain (after Dal Piaz et al., 1988) showing the main Periadriatic intrusive bodies and dikes (in black: 1, Traversella; 2, Biella; 3, Novate; 4, Bergell; 5, Adamello; 6, Gran Zebrù-Val della Mare-Lago Verde; 7, Rumo-Samoclevo; 8, northern Bressanone; 9, Rensen-Monte Alto; 10, Cima di Villa; 11, Vedrette di Ries; 12–15, eastern lamellae and apophyses), volcanic centres (16, Marostica Hills; 17, Mts. Lessini; 18, Mts. Berici, 19, Euganean Hills), and the sampled areas (in light grey: (A) Ortler-Cevedale and Ulten, Central Alps; Rabby, Sole and Rendena Valleys, western branch of the Judicarian Line; (B) Sarca and Adige Valleys, south of the Judicarian Line).

event is mainly Oligocenic in age (32–30 Ma), some intrusives of the Adamello batholith (Re di Castello and Corno Alto plutons) are significantly older (42–39 Ma) (Borsi et al., 1979; Del Moro et al., 1983; Hansmann et al., 1983; Macera et al., 1983).

On the other hand, a within-plate volcanism of Paleocene-Oligocene age took place in the Eastern Alps foreland (the Peri-Alpine domain), specifically on the Veneto region (cf. Macera et al., 2003a and references therein). Over a time span of 30–35 million years, from late Paleocene to late Oligocene, with minor magmatic events occurring during the early Miocene, four main volcanic centres developed in the Veneto region, together with numerous mafic dikes of basaltic composition (Fig. 1).

The orogenic (calc-alkaline) suite consists of several plutonic bodies of variable size, numerous andesitic, shoshonitic and ultrapotassic dikes and minor volcanics and volcanoclastic sequences. From west to east, the main intrusive bodies are represented by Biella, Traversella and Miagliano plutons in the Western Alps; Adamello, Bergell and Ortler-Cevedale massifs in the Central Alps; and Rensen, Monte Alto, Rio Vena, Vedrette di Ries and Cima di Vila on the Eastern Alps (Fig. 1). All of them share a prevailing Tonalitic–Trondhjemitic–Granodioritic composition (TTG), but minor granitic and dioritic apophyses are also present, especially at the borders of the plutons. The subvolcanic dikes range in composition from K-rich alkali-basalts to calc-alkaline basalts and shoshonites. Plutons emplacement is dated at middle Oligocene (30–31 Ma) (Borsi et al., 1979; Del Moro et al., 1983; Barth et al., 1989). The subvolcanic activity started at the same time but continued up to Late Oligocene (24 Ma; Deutsch, 1984).

The anorogenic suite consists mainly of Na-rich alkaline basalts, basanites, and transitional basalts, while hawaiites, trachybasalts, tephrites, basaltic andesites and differentiated rocks are either missing or scarce (De Vecchi and Sedea, 1974, 1995). The magmatism developed discontinuously from late Paleocene to late Oligocene, giving rise to the four main magmatic centers (Lessini, Berici, Euganei and Marostica in the Veneto region) and to numerous mafic dikes in the Perialpine domain (SE of the Judicarian Line, between Val di Sarca and Val D'Adige; Fig. 1) of late Paleocene-Middle Eocene age (Castellarin and Piccoli, 1966; Luciani, 1989). The climax of the volcanic activity occurred in the middle Eocene.

The alkaline basalts and basanites are characterized by HIMU-OIB (High μ = high $^{238}U/^{204}Pb$-Ocean Island Basalts) geochemical signatures, even if more or less diluted by a depleted MORB mantle (DMM) component (Macera et al., 2003a). They predate by only a few million years the widespread calc-alkaline magmatism that developed in the proximity of the Periadriatic Lineament: the oldest products of the Adamello batholith (Re di Castello gabbros) were dated at 42 Ma (Del Moro et al., 1983).

The development of the two contrasting magmatic suites in the Alpine area, e.g. the orogenic, mainly felsic, calc-alkaline to shoshonitic suite of Eocene-Oligocene age (42–30 Ma) which outcrops close to the Periadriatic Lineament, and the anorogenic

mafic alkaline volcanic suite which developed discontinuously from late Paleocene to Oligocene (58–30 Ma) in the Perialpine area (South Eastern Alps Volcanics, SEAV) (De Vecchi and Sedea, 1995; Milani et al., 1999; Beccaluva et al., 2000; Macera et al., 2003a), is an intriguing feature of the Tertiary magmatism in the Alps. Besides, it is noticeable that concomitant occurrence of both subduction-related and within-plate magmas in the same tectonic environment dominated by collision processes is not a unique feature of this area (cf. e.g. Bonin, 2004), but represents a widespread phenomenon in the whole Mediterranean area during tertiary–quaternary time.

A progressive transition with time from calc-alkaline to Na-rich alkaline products has been noticed in many European and northern Africa centres, such as eastern and southern Spain, Sardinia, southern Italy, Romania, Pannonian Basin, Morocco, Tunisia, Turkey (Szabo et al., 1992; Downes et al., 1995a,b; Dobosi et al., 1995; Cebria and Lopez-Ruiz, 1995; Rosembaum et al., 1997; El Bakkali et al., 1998; Wilson and Bianchini, 1999; Aldanmaz et al., 2000; Cebria et al., 2000; Harangi, 2001; Coulon et al., 2002; Gasperini et al., 2002; Duggen et al., 2005), where compressive phases alternated with tensional phases. The latter were responsible for the Cenozoic rift system of eastern and Central Europe ("ECRIS"; Ziegler, 1992), as well as for the formation of new oceanic basins, such as the Alboran Sea, the Valencia Trough, the Algero-Liguro-Provencal and the Tyrrhenian basin, from early Eocene to late Miocene (see e.g. Docherty and Banda, 1995; Faccenna et al., 1997).

The development of Na-rich alkaline basalts, typically HIMU-DMM, in most of the above-mentioned areas often affected by previous subduction episodes has been interpreted in different ways, i.e.: (i) occurrence of an extended low-velocity layer with common anomalous DMM-HIMU composition beneath Europe (Wilson and Downes, 1991; Hoernle et al., 1995; Jung and Hoernes, 2000; Harangi et al., 2003; Gasperini et al., 2003), (ii) intrusion of hot mantle fingers beneath the rift areas (Granet et al., 1995; Wilson and Patterson, 2002), (iii) upwelling of enriched asthenospheric mantle after the detachment of the subducted slab (Keskin, 2003; Harangi, 2004), (iv) upwelling of a deep mantle component through a plate window generated after a slab breakoff (Albarède et al., 2000; Gasperini et al., 2002; Macera et al., 2003a). In the Veneto Volcanic Province, the occurrence of within-plate basalts of Tertiary age having HIMU-DMM signatures has been ascribed to upwelling of plume-like mantle diapirs taking place before the subducting slab crossed the upflow of plume material or, later on, through a plate window generated after Alpine slab breakoff (Macera et al., 2003a; Ranalli et al., 2004).

To check the latter suggestion and to examine the possible genetic relations between the two contrasting magma suites, we combine the geochemical and isotopic data (Sr, Nd and Pb) on the most primitive magmatic products belonging to the two suites with a semi-quantitative assessment of the rheological behaviour of an oceanic and partly continental slab during subduction. We present new geochemical data, estimate the time evolution of negative buoyancy of an initially mature slab subducting at a dip angle of 45° with two different subduction histories, evaluate the slab softening effect of contact with plume material, and estimate the likelihood and timing of the Alpine slab detachment.

2. Sample description

Fourteen selected calc-alkaline dikes among the most undifferentiated rocks from the Central Alps (Ortler-Cevedale and Ulten Valley) and the western branch of the Judicarian Line (between the Rabby Valley and the Sole Valley, and on Rendena Valley), and 18 alkaline dikes from the eastern branch of the South Judicarian Line (Val di Sarca and Val D'Adige; see Fig. 1 for sample location) have been analyzed for major and trace elements and Sr and Nd isotope compositions.

Most of the calc-alkaline samples are porphyritic trachybasalts or trachy-andesites with plagioclase and hornblende as the main mineral phases. The groundmass is microcrystalline or crystalline. The alkaline dikes are fine-grained hypocrystalline or porphyritic basalts and basanites with scant amounts of glass. The groundmass is generally microcrystalline, with olivine, clinopyroxene and plagioclase being the main mineral phases. Nepheline and variable amounts of oxides may be also present. Major and trace element data on the mafic dikes from the two suites are shown in Table 1.

Table 2 lists Sr and Nd isotope data for the same samples. These data are discussed together with geochemical and Sr-, Nd- and Pb-isotope data from the literature in order to obtain a more complete picture of Alpine magmatism.

Major element concentrations were determined by XRF at the University of Pisa Earth Sciences Department, following the analytical procedures of Franzini et al. (1975) and Leoni and Saitta (1976), while trace element analyses were carried out at the C.R.P.G. in Nancy (Centre de Recherches Pétrographiques et Géochimiques, Service d'Analyse des Roches et des Minéraux du C.N.R.S.; Alibert et al., 1983). Precision for the trace element analyses is 5–20% at the 1 ppm level, 2–10% at the 10 ppm level, and 2–5% at the 100 ppm level. Ferrous/ferric iron ratios were determined by titration. Sr and Nd isotopic compositions were analyzed by the multi-collector Finnigan Mat 262 mass spectrometer at the I.G.G.-C.N.R. facility in Pisa (Istituto di Geoscienze e Georisorse del C.N.R., Pisa), following the elemental separation procedure of Clocchiatti et al. (1994).

Total procedural blanks for Sr and Nd were better than 2 ng. Sample to blank ratios for the two elements for all samples analyzed were $\gg$1000. Uncertainties reported on Sr and Nd measured isotope ratios are $2\sigma/n^{1/2}$ analytical errors in the last decimal place, where n is the number of measured isotope ratios. $^{87}Sr/^{86}Sr$ of the NBS-987 Sr standard = 0.710226 ± 12 ($n = 11$); $^{143}Nd/^{144}Nd$ of the La Jolla Nd standard = 0.511855 ± 5 ($n = 12$). $^{87}Sr/^{86}Sr$ and $^{143}Nd/^{144}Nd$ were normalized for mass fractionation relative to $^{86}Sr/^{88}Sr = 0.1194$ and $^{146}Nd/^{144}Nd = 0.7219$, respectively.

3. Geochemical features of orogenic and anorogenic suites

The calc-alkaline magmas (TTG and dikes) from the Western, Central and Eastern Alps share comparable geochemical

Table 1
Major and trace element composition for calc-alkaline and alkaline dikes from Central and Eastern Alps

Sample	Calc-alkaline rocks													
	FP239	FP53	FP40	FP16	FP94	FP21	FP461	FP460	FP456	FP415	FP297	FP350	FP360	FP549
SiO_2	54.57	45.94	50.88	52.71	53.96	55.74	52.35	50.55	52.57	54.42	44.56	64.28	46.50	59.03
TiO_2	0.88	1.35	0.82	0.78	0.62	1.12	1.00	1.02	1.07	0.95	2.64	0.44	2.31	0.60
Al_2O_3	14.65	18.86	19.69	14.89	18.98	16.69	17.06	16.23	16.40	16.85	13.21	17.20	11.12	18.38
Fe_2O_3	3.87	4.14	2.62	1.90	3.44	1.77	1.06	1.77	3.76	2.35	5.74	1.67	4.94	3.72
FeO	4.13	7.62	5.14	6.76	4.07	4.83	5.95	5.60	3.41	4.20	6.52	2.03	6.76	1.87
MnO	0.12	0.18	0.16	0.21	0.15	0.12	0.13	0.12	0.12	0.10	0.16	0.09	0.26	0.13
MgO	4.51	5.60	3.89	6.73	4.15	4.96	7.61	9.19	5.81	6.54	9.91	2.04	11.15	1.88
CaO	5.92	8.99	8.62	8.36	9.00	7.10	5.94	7.73	10.16	6.71	9.25	4.45	10.51	6.84
Na_2O	2.44	2.39	3.49	2.27	2.69	3.89	3.73	2.96	3.93	3.70	2.92	4.37	2.11	2.64
K_2O	4.42	2.58	2.81	3.10	0.97	1.35	1.16	1.06	0.28	1.50	1.71	2.17	1.02	2.04
P_2O_5	0.77	0.54	0.44	0.27	0.13	0.21	0.20	0.16	0.22	0.17	0.86	0.16	0.47	0.29
LOI	3.38	0.93	0.84	1.22	1.23	1.53	3.05	2.90	1.78	1.93	1.61	0.90	2.58	2.26
Total	99.66	99.12	99.4	99.2	99.39	99.31	99.24	99.29	99.51	99.42	99.09	99.8	99.73	99.68
V	195	350	196	183	189	139	159	171	184	154	225	91	224	64
Cr	92	19	38	328	126	151	397	527	371	324	259	158	481	231
Co	21	47	30	27	20	42	27	28	24	27	46	6	58	9
Ni	25	16	19	104	26	40	150	187	96	121	190	22	344	n.d.
Rb	155	156	147	166	34.4	48.4	48.4	46.9	8.5	70.5	88.3	74.7	36.7	94.5
Sr	1080	791	903	540	295	352	406	431	751	424	851	959	587	675
Ba	1947	941	826	776	185	204	346	228	108	341	2216	1396	510	266
Cs	4.11	10.7	7.74	9.75	5.13	1.88	1.65	1.73	0.2	2.18	9.57	3.81	2.1	4.24
Y	24.9	27.9	26.4	29.3	18.5	27.4	18.0	15.6	17.7	18.1	28.6	12.5	24.9	23.2
Zr	213	162	183	83	74	173	125	96	108	118	185	109	161	185
Hf	5.87	4.06	4.56	2.47	2.12	4.37	3.65	2.9	3.08	3.57	4.29	3.15	4.13	5.06
Nb	14.1	13.0	12.2	13.4	3.50	6.81	9.34	7.17	15.4	9.25	30.3	19	21.0	11.6
Ta	1.18	1.55	1.46	0.94	0.27	0.96	1.08	0.86	1.05	1.01	1.6	1.72	1.29	0.88
Pb	14.8	9.50	12.8	12.0	3.23	12.2	20.2	25.1	14.8	16.3	31.4	36.6	22.1	17.2
La	54.5	39.1	33.1	26.6	8.67	17.8	24.5	18.2	19.8	29.5	128	39.2	65.5	38.4
Ce	112	87.0	73.3	66.4	19.2	39.9	47.5	36.2	41.8	58.6	228	65.9	123	75.4
Pr	12.9	10.3	9.07	8.76	2.49	5.16	5.60	4.41	5.66	7.32	24.0	6.47	13.4	8.76
Nd	52.8	41.9	38.6	36.6	11.1	21.6	22.9	18.1	23.5	28.3	89.9	22.9	52.2	31.6
Sm	10.2	8.28	7.82	8.06	2.91	5.16	4.41	4.00	5.48	5.34	14.5	3.84	9.90	5.97
Eu	2.37	2.01	1.93	1.94	0.93	1.45	1.13	1.08	1.47	1.25	4.00	1.13	2.67	1.53
Gd	7.50	6.78	6.58	6.53	2.85	4.99	4.00	3.40	4.81	4.72	10.4	2.95	7.90	4.48
Tb	1.01	0.92	0.88	0.95	0.49	0.79	0.59	0.54	0.71	0.66	1.32	0.42	1.08	0.70
Dy	5.23	5.35	4.97	5.51	2.82	4.66	3.40	2.98	4.00	3.80	6.23	2.49	5.04	3.79
Ho	0.90	1.02	0.99	1.12	0.65	1.10	0.69	0.62	0.74	0.69	1.08	0.42	0.93	0.82
Er	2.53	2.95	2.63	2.92	1.98	2.63	1.86	1.57	1.72	1.81	2.68	1.22	2.12	2.19
Tm	0.33	0.39	0.37	0.44	0.29	0.37	0.26	0.24	0.27	0.26	0.32	0.19	0.32	0.36
Yb	2.18	2.73	2.28	2.86	2.01	2.47	1.79	1.55	1.71	1.65	1.99	1.37	1.83	2.43
Lu	0.35	0.47	0.37	0.51	0.33	0.43	0.29	0.23	0.24	0.27	0.25	0.22	0.27	0.39
U	10.3	2.14	4.15	3.52	0.41	1.70	4.78	3.19	1.29	3.84	5.89	9.00	3.48	2.05
Th	25.9	5.81	11.7	12.9	2.00	4.88	11.1	7.58	4.48	8.42	34.3	16.1	18.6	11.4

Table 1 (*Continued*)

Sample	Alkaline rocks																	
	K7	K8	K11	K 51-2	K 51-3	K 55-1	K 55-2	K 56-1	K 57-1	K 57-3	K 62-1	K 70-1	K70-3	53 C	54 B	67	96	113
SiO_2	41.79	42.12	48.20	37.39	39.77	35.79	35.20	44.41	35.74	38.38	39.94	38.92	35.26	39.50	36.63	44.72	44.37	44.08
TiO_2	2.96	3.05	1.84	2.07	2.22	2.28	2.16	2.05	2.87	3.13	2.39	2.28	1.93	2.30	2.10	3.35	3.17	3.08
Al_2O_3	13.67	13.48	14.32	10.66	11.17	11.05	11.13	13.92	10.94	10.06	13.21	11.34	10.68	11.08	10.48	13.95	14.10	14.49
Fe_2O_3	4.96	4.16	3.42	4.35	4.40	6.29	5.61	3.87	6.96	5.76	5.09	2.29	5.41	7.38	7.62	5.73	6.49	3.94
FeO	7.59	8.53	7.52	5.00	6.55	4.92	5.18	4.74	5.96	5.49	5.76	5.90	3.84	3.59	3.00	5.69	4.88	7.97
MnO	0.19	0.18	0.13	0.12	0.15	0.18	0.18	0.12	0.15	0.14	0.17	0.10	0.14	0.16	0.18	0.14	0.18	0.18
MgO	8.13	8.90	7.99	19.40	14.59	14.02	13.98	7.03	10.20	17.11	13.35	22.31	22.83	15.80	12.70	6.40	8.50	8.26
CaO	10.46	10.92	8.77	8.81	10.43	15.21	15.24	13.01	15.32	8.91	9.70	7.44	9.88	9.74	16.23	10.03	9.35	9.38
Na_2O	3.89	3.36	2.82	0.75	1.52	0.92	1.09	4.11	3.25	1.54	1.23	2.55	0.87	1.90	1.38	2.52	4.17	3.44
K_2O	1.98	1.82	0.90	0.90	1.18	0.66	0.97	1.45	2.06	1.12	1.92	1.58	0.35	0.30	0.61	2.19	1.28	2.03
P_2O_5	1.42	1.05	0.38	0.99	1.08	1.85	1.82	0.88	0.93	1.30	1.28	0.84	1.38	1.83	1.39	1.16	0.87	1.39
LOI	1.56	1.52	2.78	9.57	6.94	6.83	7.43	4.40	5.61	7.05	5.96	4.44	7.44	6.43	7.68	4.11	2.64	1.75
Total	98.60	99.09	99.07	100.01	100.00	100.00	99.99	99.99	99.99	99.99	100.00	99.99	100.01	100.01	100.00	99.99	100.00	99.99
V	220.32	235.09	178.05	192.71	196.79	198.59	200.16	144.43	186.59	237.34	232.98	255.52	206.03	203.43	195.22	214.78	243.13	220.29
Cr	242.11	339.94	401.27	249.80	330.89	297.32	296.56	204.99	86.59	176.38	233.04	251.03	209.55	344.52	392.71	94.23	168.06	183.85
Co	43.91	49.22	50.57	41.28	48.57	46.89	46.17	33.45	38.68	48.89	44.29	54.53	47.46	50.40	46.55	41.46	45.63	48.41
Ni	124.27	162.50	238.71	172.01	218.05	221.18	221.37	128.49	81.24	146.66	146.07	207.21	191.16	254.38	232.96	95.83	148.16	147.39
Rb	22.43	40.03	20.69	15.57	24.02	17.27	23.41	36.83	39.78	23.02	35.23	26.77	10.74	10.53	21.10	48.33	33.30	48.17
Sr	1120.22	1247.00	426.54	248.32	481.26	1099.21	1266.80	996.36	563.45	483.28	676.47	748.98	553.71	686.57	1291.13	1103.11	1134.76	1066.56
Ba	719.66	628.04	226.82	797.34	366.94	676.92	925.76	552.84	599.82	523.38	695.50	469.57	570.18	485.43	910.64	2174.26	677.80	632.25
Cs	2.76	0.47	<L.D.	0.40	0.36	0.67	0.72	0.58	1.11	0.42	0.67	0.73	<L.D.	0.24	2.57	0.53	0.82	0.76
Y	32.15	31.85	21.07	22.21	25.08	31.65	32.35	22.95	24.74	24.81	28.72	24.77	30.92	32.34	31.66	28.88	30.48	30.77
Zr	356.72	289.37	129.45	196.83	212.78	267.44	267.86	258.99	299.09	253.36	232.37	262.71	287.87	266.18	257.80	389.78	376.84	324.10
Hf	7.07	6.20	3.36	4.43	4.83	5.20	5.03	5.76	6.74	5.70	4.81	5.89	5.33	5.13	4.98	8.47	8.38	7.00
Nb	98.67	66.35	23.34	41.90	45.39	66.38	86.00	54.89	49.86	53.98	61.44	58.14	66.24	69.14	68.99	78.57	84.21	73.56
Ta	6.52	4.41	1.63	2.80	3.08	3.87	4.77	3.63	3.62	3.82	4.31	4.38	3.95	3.84	3.88	5.64	6.20	5.23
Pb	5.08	4.43	2.28	3.11	4.28	9.19	6.88	2.61	4.06	3.14	5.46	3.81	3.94	6.66	4.82	4.71	4.79	5.40
La	76.69	69.74	24.10	37.50	43.14	91.85	102.63	47.68	47.32	48.21	73.88	44.86	69.81	86.74	82.03	64.65	67.32	65.31
Ce	150.86	138.55	49.10	78.10	88.68	174.40	189.92	92.93	97.57	99.37	141.61	93.35	141.49	167.23	152.66	127.76	130.28	127.95
Pr	17.51	16.13	5.81	9.82	10.89	19.94	20.90	11.43	12.49	11.94	15.64	11.18	16.38	19.41	18.08	15.67	15.69	15.63
Nd	72.17	65.70	24.96	42.15	47.13	77.71	77.72	47.31	51.63	49.21	61.25	44.42	64.29	75.75	70.36	61.64	60.74	60.67
Sm	13.75	12.37	5.57	8.76	9.82	13.82	14.23	9.39	11.21	10.30	10.96	9.13	12.36	13.90	13.28	12.09	10.90	12.08
Eu	4.28	3.93	1.85	2.82	2.97	4.30	4.36	2.93	3.56	3.25	3.47	2.77	3.95	4.51	3.97	3.78	3.58	3.61
Gd	11.48	10.25	5.47	7.80	7.82	10.92	11.22	8.55	9.85	9.11	9.73	8.54	10.55	11.39	9.95	8.94	9.31	9.49
Tb	1.45	1.34	0.76	1.04	1.17	1.49	1.60	1.09	1.27	1.18	1.29	1.13	1.43	1.47	1.39	1.31	1.25	1.29
Dy	7.04	6.69	4.03	5.00	5.90	7.36	7.24	5.10	6.12	5.67	6.26	5.31	6.57	7.21	7.03	6.81	6.65	6.53
Ho	1.21	1.14	0.81	0.79	0.87	1.06	1.18	0.75	0.97	0.90	1.06	0.93	1.11	1.13	1.13	1.02	1.12	1.00
Er	2.72	2.83	1.94	1.93	2.11	2.72	2.82	1.86	2.11	2.11	2.74	2.17	2.74	2.75	2.47	2.43	2.66	2.41
Tm	0.35	0.37	0.28	0.25	0.27	0.34	0.39	0.24	0.25	0.27	0.33	0.29	0.30	0.33	0.33	0.29	0.36	0.30
Yb	2.16	2.12	1.75	1.44	1.59	1.90	2.11	1.30	1.45	1.61	2.21	1.65	1.87	2.05	1.91	1.65	2.05	1.88
Lu	0.27	0.27	0.26	0.20	0.21	0.31	0.30	0.21	0.21	0.21	0.29	0.26	0.27	0.27	0.24	0.22	0.27	0.26
U	2.61	2.17	1.05	1.22	1.39	2.86	3.89	1.77	1.52	1.50	3.70	1.55	1.90	3.01	3.02	2.21	2.57	2.27
Th	8.97	7.40	3.64	4.17	4.56	10.03	12.52	6.05	4.84	5.26	8.68	5.34	6.62	10.63	10.02	7.64	8.59	8.49

n.d.: Not determined; <L.D.: below detection limit.

Table 2
Sr and Nd isotope compositions for the most primitive dikes from Central and Eastern Alps

Sample	Rb	Sr	$^{87}Rb/^{86}Sr$	$^{87}Sr/^{86}Sr \pm 2\sigma$	$^{87}Sr/^{86}Sr_i$	Sm	Nd	$^{147}Sm/^{144}Nd$	$^{143}Nd/^{144}Nd \pm 2\sigma$	$^{143}Nd/^{144}Nd_i$	ε_{Ndi}
Calc-alkaline rocks[a]											
FP239	155	1080	0.41	0.707631 ± 7	0.70745	10.2	52.8	0.12	0.512318 ± 12	0.51230	−6.69
FP53	156	791	0.57	0.708047 ± 6	0.70781	8.28	41.9	0.12	0.512446 ± 6	0.51242	−4.19
FP40	147	903	0.47	0.707601 ± 6	0.70741	7.82	38.6	0.12	0.512444 ± 7	0.51242	−4.25
FP16	166	540	0.89	0.707590 ± 6	0.70721	8.06	36.6	0.13	0.512460 ± 8	0.51243	−3.98
FP94	34.4	295	0.34	0.706017 ± 8	0.70587	2.91	11.1	0.16	0.512675 ± 7	0.51264	0.12
FP21	48.4	352	0.40	0.710593 ± 11	0.71042	5.16	21.6	0.14	0.512599 ± 7	0.51257	−1.31
FP461	48.4	406	0.35	0.712606 ± 8	0.71245	4.41	22.9	0.12	0.512317 ± 8	0.51229	−6.71
FP460	46.9	431	0.32	0.710175 ± 9	0.71004	4.00	18.1	0.13	0.512373 ± 6	0.51235	−5.68
FP456	8.54	751	0.03	0.708199 ± 6	0.70819	5.48	23.5	0.14	0.512534 ± 11	0.51251	−2.57
FP415	70.5	424	0.48	0.709596 ± 7	0.70939	5.34	28.3	0.11	0.512372 ± 10	0.51235	−5.62
FP297	88.3	851	0.30	0.707449 ± 7	0.70732	14.5	89.9	0.10	0.512542 ± 9	0.51252	−2.24
FP350	74.7	959	0.23	0.705233 ± 8	0.70514	3.84	22.9	0.10	0.512515 ± 8	0.51250	−2.79
FP360	36.7	587	0.18	0.707611 ± 7	0.70753	9.90	52.2	0.12	0.512577 ± 7	0.51256	−1.62
FP549	94.5	675	0.41	0.706597 ± 8	0.70643	5.98	31.6	0.11	0.512331 ± 13	0.51231	−6.42
Alkaline rocks[b]											
K7	22.4	1120	0.06	0.703282 ± 6	0.70325	13.8	72.2	0.12	0.512935 ± 6	0.51291	5.21
K8	40.0	1247	0.09	0.703226 ± 7	0.70317	12.4	65.7	0.11	0.512924 ± 6	0.51289	4.99
K11	20.7	427	0.14	0.703823 ± 8	0.70374	5.57	25.0	0.14	0.512853 ± 10	0.51282	3.51
K55-1	17.3	1099	0.05	0.703285 ± 6	0.70326	13.8	77.7	0.11	0.512918 ± 9	0.51289	4.91
K56-1	36.8	996	0.11	0.703486 ± 9	0.70343	9.39	47.3	0.12	0.512975 ± 5	0.51294	5.96
K57-1	39.8	563	0.20	0.703466 ± 6	0.70335	11.2	51.6	0.13	0.513004 ± 8	0.51297	6.47
K62-1	35.2	676	0.15	0.703692 ± 6	0.70361	11.0	61.2	0.11	0.512906 ± 1	0.51288	4.68
K70-1	26.8	749	0.10	0.703285 ± 6	0.70323	9.12	44.4	0.12	0.512940 ± 9	0.51291	5.26
53C	10.5	687	0.04	0.703184 ± 8	0.70316	13.9	75.8	0.11	0.512896 ± 12	0.51286	4.40
54B	21.1	1291	0.05	0.703263 ± 6	0.70326	13.3	70.4	0.11	0.512922 ± 1	0.51289	4.88
67	48.3	1103	0.13	0.703134 ± 6	0.70305	12.1	61.6	0.12	0.512956 ± 7	0.51292	5.52
96	33.3	1135	0.08	0.703033 ± 6	0.70298	10.9	60.7	0.11	0.512939 ± 8	0.51291	5.25
113	48.2	1067	0.13	0.703239 ± 6	0.70316	12.1	60.7	0.12	0.512928 ± 6	0.51289	4.97

Rb, Sr, Sm and Nd are in ppm.
[a] 30–32 Ma old.
[b] 40–45 Ma old.

patterns that are characterized by a progressive increase of the most incompatible elements and peculiar troughs at Nb, Ta, Ti, and peaks at Th, U, K and Pb (Fig. 2a). These patterns are typical of subduction-related magmas (Thorpe et al., 1984; Hickey et al., 1986). Moreover, a different trace element enrichment among TTG and calc-alkaline dikes from the Western, Central and Eastern Alps is highlighted in Fig. 2a. This variation in trace element abundances is associated to variable light rare earth/heavy rare earth element fractionations ($5 < (La/Yb)n < 46$) and can be related to different degrees and depths of partial melting of a heterogeneous mantle source (Deutsch, 1984; Bellieni et al., 1991, 1996; Macera et al., 1998).

The SEAV (alkaline suite) show geochemical patterns typical of ocean island basalts (OIB), e.g. a progressive increase of the most incompatible trace elements up to Ta, negative spikes at Pb and a progressive decrease of the normalized-abundance from Nb to Cs (Fig. 2b). These features are comparable to those of tertiary–quaternary HIMU-OIB basalts from the western Mediterranean area (Gasperini et al., 2003; Macera et al., 2004).

Additional evidence for the contrasting geochemical features of the alkaline and calc-alkaline suites is provided by variations of incompatible element ratios and Sr–Nd–Pb isotope compositions. The most primitive Periadriatic magmas are characterized by incompatible element ratios that are quite similar to those of subduction-related lavas (VAB in Fig. 2c–e). By contrast, the SEAV show distinctly lower Rb/Nb, Zr/Nb, La/Nb and Th/Ta ratios, and higher Nb/U and Ta/Yb ratios than the Periadriatic intrusions and dikes (Fig. 2c–e), features that they share with the Mediterranean HIMU basalts. The relative contribution of a subduction-related versus an OIB-related component in the Alpine magmas is particularly evident in Fig. 2c and d where, on average, Western Alps samples are characterized by the highest Th/Ta and the lowest Nb/U ratios (strongest subduction hallmark), and the SEAV by the lowest Th/Ta and highest Ta/Yb ratios (strongest HIMU hallmark). The SEAV also show higher initial ε_{Nd} (+3.5 to +6.8) and $^{206}Pb/^{204}Pb$ (18.786–19.574), and lower $^{87}Sr/^{86}Sr$ (0.70298–0.70374) ratios than the Periadriatic magmas ($\varepsilon_{Nd} = +3.18$ to -8.48, $^{206}Pb/^{204}Pb = 18.6490–18.7801$, $^{87}Sr/^{86}Sr = 0.70389–0.71257$; data from Macera et al., 2003a; Gasperini et al., 2006 and this work).

In Sr–Nd and Sr–Pb isotope space (Fig. 3a and b) the two suites define a mixing trend, the two end members being the SEAV component and a continental crust component, namely the lower continental Calabrian crust (LCCC; data from Caggianelli et al., 1991). Results obtained by performing mixing calculations (Langmuir et al., 1978) on Sr, Nd and Pb isotopes support these hypotheses (details in Fig. 3). In particular, the most primitive basalts of SEAV show isotopic features that are compatible with

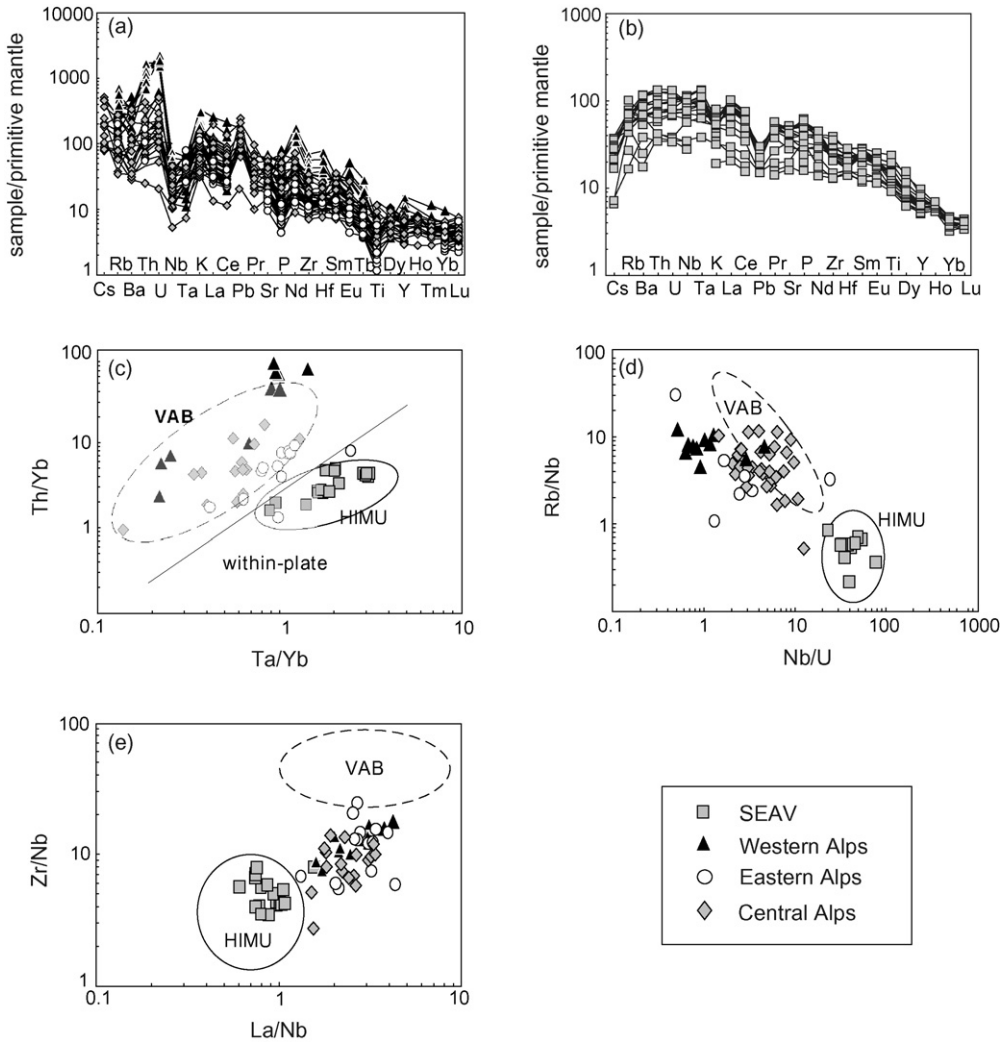

Fig. 2. (a) Primitive mantle-normalized (GERM, http://www.earthref.org/) incompatible element-spider diagrams for the Periadriatic magmas (data from Bellieni et al., 1991, 1996; Macera et al., unpublished, 2006, and this work), and (b) SEAV (data from Macera et al., 2003a, and this work); (c) Th/Yb vs Ta/Yb ratios, (d) Rb/Nb vs Nb/U ratios, and (e) Zr/Nb vs La/Nb ratios for SEAV along with data for Mediterranean HIMU basalts and volcanic arc basalts (from http://georoc.mpch-mainz.gwdg.de/Start.asp). Most of SEAV show incompatible element ratios similar to Mediterranean HIMU basalts. Field of VAB and within-plate basalts from Peccerillo (2003, 2005).

a mixture of about 40% HIMU and 60% DMM. Conversely, the isotope compositions of the more evolved magmas of both SEAV and Periadriatic magmatism can be obtained by variable proportions of this HIMU-DMM component and the LCCC component. The choice of Calabrian-type lower crust as a potential end member of the alkaline and calc-alkaline magma mixing in the Alpine area derives from geological and geochemical considerations. The lower Calabrian crust corresponds to the base of the highest nappe of the Cretaceous-Paleogene pile (Del Moro et al., 1986) which according to many authors can be considered as an extension of the Alps (Alvarez, 1976; Amodio-Morelli et al., 1976; Bonardi et al., 1982).

In summary, SEAV isotope characteristics are compatible with a mixture of a diluted HIMU-DMM component with a maximum of 10% of LCCC material, likely occurred during the magma ascent; by contrast those of the Periadriatic magmas are compatible with a mixture of the SEAV component with approximately 10%, up to 60% of LCCC (for mixing parameters, see caption of Fig. 3).

4. Relationships between alkaline and calc-alkaline magmas

The occurrence of subduction- and plume-related (OIB) magmas in the same collisional environment such as the Alpine domain during the tertiary has important geodynamic implications.

At present, there is no indication of a hot spot under the South-Eastern Alps. Seismic tomographic data show a low-velocity anomaly in the upper mantle extending down to 400 km, while flat-lying high-velocity material is found in the mantle transition zone (Piromallo and Faccenna, 2004). This material is interpreted as the Paleogene subducted lithosphere, detached by an event occurring around 35–30 Ma (Piromallo

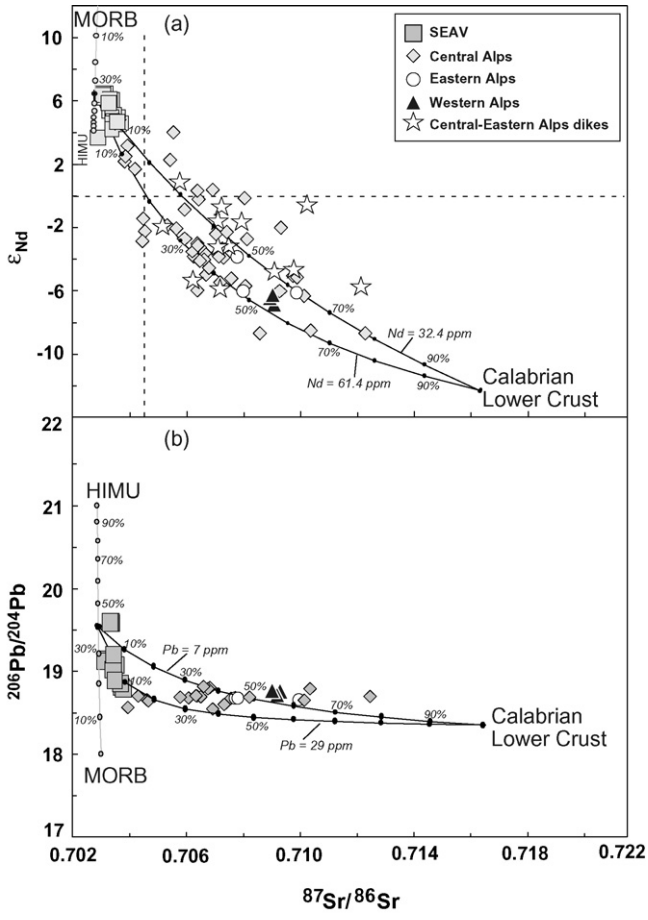

Fig. 3. (a) Sr–Nd and (b) Sr–Pb isotope variation for SEAV and Periadriatic magmas. Mixing relationships between SEAV and a lower continental crust (Caggianelli et al., 1991), have been checked by performing mixing calculations (Langmuir et al., 1978) on Sr, Nd and Pb isotopes. The most primitive basalts of SEAV show isotopic features that are compatible with a mixture of about 40% HIMU and 60% DMM. Variable proportions of this HIMU-DMM component and a continental crust-derived end-member can account for the isotopic variability of most of the investigated magmas. SEAV isotope peculiarities are compatible with a mixture of a diluted HIMU component with a maximum of 10% lower continental crust in their mantle source, while those of the Periadriatic magmatism may reflect 10–60% anatexis of the lower continental crust. Geochemical data for HIMU-DMM and the Calabrian lower continental crust are arithmetic average values calculated on the GEOROC database (http://georoc.mpch-mainz.gwdg.de/Start.asp) and from Caggianelli et al. (1991), respectively. DMM: $^{87}Sr/^{86}Sr = 0.7030$; $^{143}Nd/^{144}Nd = 0.51330$; $^{206}Pb/^{204}Pb = 18.00$; Sr = 137 ppm; Nd = 11.6 ppm; Pb = 2 ppm; HIMU: $^{87}Sr/^{86}Sr = 0.70285$; $^{143}Nd/^{144}Nd = 0.51285$; $^{206}Pb/^{204}Pb = 21.00$; Sr = 376 ppm; Nd = 49.2 ppm; Pb = 3 ppm; Calabrian crust: $^{87}Sr/^{86}Sr = 0.71681$; $^{143}Nd/^{144}Nd = 0.51201$; $^{206}Pb/^{204}Pb = 18.358$; Sr = 239 ppm. For the Calabrian lower crust, Nd (32.4–61.4 ppm) and Pb (7–29 ppm) concentrations chosen to calculate mixing relationships fall within the range of variation for this component (Pb = 1.5–29.0 ppm; Nd = 5.2-61.4; Caggianelli et al., 1991). On the mixing lines, black dots and relative labels correspond to different proportions of (a) the HIMU component in the HIMU-DMM mixing, and (b) the crustal component in the HIMU-DMM-crust mixing (in this case, the mixture HIMU-DMM is fixed at 40–60%, respectively. See text for further details). Sr and Nd isotope data for SEAV and Periadriatic magmatism from Macera et al. (2003a), Gasperini et al. (2006), and this work; Pb isotope data from Juteau et al. (1986), Bellieni et al. (1996), Barth et al. (1989), and Macera et al. (2003a).

and Faccenna, 2004). By contrast, the low-velocity anomaly has been ascribed to mantle upwelling of possibly deep origin (Macera et al., 2003a). This scenario is only a working hypothesis for within-plate volcanic centres showing small eruption volumes, discontinuous magma production, and lack of well-defined hotspot tracks. Nevertheless, the possibility of occurrence of several weaker and smaller plumes, in addition to major hotspot centres, lately has gained increasing consensus (i.e. Dalrymple et al., 1987; Malamud and Turcotte, 1999; Davis et al., 2002). Several studies based on tomographic images and geochemical data proposed the existence of small intra-continental magmatic fields fed by mantle upwelling. An interesting example is given by the numerous Cenozoic volcanic centres of Central Europe for which an origin from a series of individual diapir-like mantle upwelling has been suggested, rising either from the top of a continuous layer (fossil plume-head?) within the upper mantle (Wilson and Downes, 1991; Granet et al., 1995; Hoernle et al., 1995; Vaselli et al., 1995; Rosembaum et al., 1997; Jung and Hoernes, 2000) or from a deeper mantle reservoir (Goes et al., 1999; Ritter et al., 2001). In this context, the SEAV could represent the shallow expression of mantle upflow. A detailed discussion on a possible plume-related origin for the upper mantle low-velocity anomaly under the SEAV region is given in Macera et al. (2003a).

In addition, recent studies on tertiary–quaternary alkaline basalts from the eastern Atlantic (Serra de Monchique-Mt. Ormonde, Madeira, Canary and Cape Verde Islands), northern Africa (Morocco, Algeria, Tunisia), and Central Europe (French Massif Central in France, Rhon and Eifel in Germany, Stiria and Burgenland in Austria, Silesia in Poland, Nògrad in Czech Republic, Buda Mts in Hungary, Etna and Iblean in Italy) seem to indicate a common mantle reservoir with a typical DMM-HIMU geochemical signature beneath the entire area (Hoernle et al., 1995; Gasperini et al., 2003; Macera et al., 2004). Such a reservoir has been interpreted as the head of a mantle plume whose tail may be located in correspondence of the Cape Verde–Madeira–Canary Islands region (Gasperini et al., 2003; Macera et al., 2004). Based on geochemical, geological and geophysical data, Gasperini et al., 2003; Macera et al. (2004) suggested that the large-scale swell of the plume was frayed by the Eurasian plate while the latter was moving towards the northeast, and that plume material has been trapped in the sublithospheric mantle by flat-lying detached slabs above the transition zone. At different points in time, local extensional tectonics and slab detachment may favor plume-related volcanism, even in areas dominated by plate convergence and subduction.

5. Models for slab detachment

Slab detachment and upwelling of sub-litospheric enriched mantle material through a plate window may be a plausible mechanism for plume-related magmatism in subduction zones and for the relatively concomitant occurrence of alkaline and calc-alkaline magmas in the same region, as already proposed by several authors (El Bakkali et al., 1998; Aldanmaz et al., 2000; Albarède et al., 2000; Coulon et al., 2002; Keskin, 2003; Harangi, 2004). Other models to account for the transition

from subduction-related to intraplate-type magmatism in post-collisional environments such as the western Mediterranean in the Miocene-Pliocene invoke continental edge delamination of the subducting lithospheric slab and subsequent upwelling of plume-contaminated sub-lithospheric mantle (Duggen et al., 2005). This model, however, cannot be applied in our case because the initiation of intraplate-type magmatism predates the calc-alkaline magmatism.

In the present case, the geochemical characteristics of SEAV have been attributed to blobs of deep mantle material (the HIMU component) which rose through a lithospheric gap, attained shallower depths, and triggered partial melting of both the plume component by adiabatic decompression and the surrounding asthenospheric mantle, giving rise to the HIMU-DMM lavas of SEAV (Macera et al., 2003a). Alternatively, the SEAV could have been generated by local upwelling of the HIMU-DMM plume head, at present located in the upper mantle above the transition zone, after slab detachment. Counterflows of plume material may also have swerved to the top of the subducting slab and conductively heated the overriding mantle wedge to the point of favouring partial melting in it and subsequent mixing of magmas, as suggested by Sr-, Nd- and Pb-isotope variations in Fig. 3a and b.

A slab breakoff event in the Alpine area was first proposed by Dal Piaz and Gosso (1994) (see also von Blankenburg and Davies, 1995; Marchant and Stampfli, 1997) to explain the genesis of the Periadriatic magmatism, and it is in agreement with the rapid uplift of HP (high-pressure) mantle wedge material and the variation of the thermal regime in the western Alps since the late Eocene (Dal Piaz et al., 2001, 2003). Moreover, Piromallo and Faccenna (2004) presented further evidence for European slab breakoff through a combined tomographic study of the mantle beneath the Alpine area, geological evidence, and plate kinematics.

To test the likelihood and timing of breakoff of the European slab, we estimate the time evolution of negative buoyancy of a subducting slab, and evaluate the slab softening effect of contact with plume material. Only a few test-cases are shown to provide first-order constraints for the relevant processes and an assessment of the hypothesis that slab breakoff and type of magmatism may be related. Several quantitative models of slab breakoff exist (cf. e.g. Wong et al., 1997; Van de Zeedde and Wortel, 2001; Gerya et al., 2004), but they do not take into account the softening effect of slab–plume interaction.

The model is an adaptation of that presented in Ranalli et al. (2000) and Mahatsente and Ranalli (2004), where subduction of an oceanic slab is modelled *ab initio*. Mass, momentum, and energy conservation equations are solved for a slab and surrounding mantle subject to kinematic boundary conditions (time-dependent subduction rate, subduction dip angle and initial temperature distribution of subducting slab). The temperature within the slab (the result of combined advection and diffusion) is obtained as a function of time since the beginning of subduction. The time-dependent density anomalies within the slab are computed from the temperature distribution at each time step, taking into account phase transitions and their estimated displacement within the slab. The total buoyancy is obtained from the density anomalies by integration (for details see Mahatsente and Ranalli, 2004). This model has been extended to subduction of continental lithosphere (Ranalli et al., 2005), assuming that continental material arrives at the subduction zone at a specified time after the beginning of subduction. The resulting total buoyancy (algebraic sum of negative thermal buoyancy due to temperature anomalies, positive and negative buoyancies related to phase changes, and positive compositional buoyancy of the continental crust) is obtained as a function of time since the beginning of subduction.

Figs. 4 and 5 show the time evolution of negative buoyancy for an initially mature (age >50 Ma) slab subducting at a dip angle of 45° with two different subduction histories. The oceanic lithosphere is assumed to consist of a 7-km thick crust overlying a 93-km thick lithospheric mantle; the continental lithosphere consists of a 35-km thick crust overlying a 65-km thick mantle lid. The width of the passive continental margin (the distance over which the crust changes from oceanic to continental thickness) is taken as 150 km. For constant subduction rate (Figs. 4a–c), the negative buoyancy of an oceanic slab tends to an asymptotic value of 3.0×10^{13} to 5.5×10^{13} N m^{-1} (larger for faster subduction rates) as the slab reaches the bottom of the mantle transition zone (the further small increase in the lower mantle is neglected since it is very poorly constrained). Subduction of continental material is assumed to begin when the tip of the oceanic slab has reached the bottom of the mantle transition zone, i.e., approximately 19, 27 and 37 Ma after the initiation of subduction for the chosen velocities. If eclogitization of the continental crust does not take place, subduction of continental material decreases the overall buoyancy at a rate proportional to the subduction rate, and reduces it to negligible values in approximately 10–20 Ma. For time-dependent subduction rates (increasing exponentially during the first 5 Ma, constant at a peak value for the following 15 Ma, then decreasing exponentially over 12 Ma, and zero afterwards; Figs. 5a–c), the maximum negative buoyancy of an oceanic slab (in the range 2.5×10^{13} to 4.5×10^{13} N m^{-1}) is reached 5–10 Ma after the rate has begun decreasing. This is a consequence of the interplay between the mechanical characteristic time (depending on the subduction rate) and the thermal characteristic time (depending on the rate of heat diffusion). Subduction of continental material, assumed in this case to begin 20 Ma after the initiation of subduction independent of the peak subduction rate, reduces by about 10 Ma the time required to bring the overall buoyancy to negligible values.

The geometry for the calculation of the plume effect is shown in Fig. 6. A time-dependent subduction rate with peak velocity 3.5 cm a^{-1} (see Fig. 5b) is adopted. The slab is 100 km thick, dips at an angle of 45°, and has an overall downdip length of 600 km (measured on its lower boundary from the bending point). Continental crust is assumed to have been subducted to point C, corresponding to a downdip length of 300 km measured from the bending point. In terms of depth, the tip of the slab has reached a depth of ∼525 km, and the continental material a depth of ∼240 km. Subduction of continental material to depths of this order is mechanically feasible (Ranalli et al., 2000) and is proven by the occurrence of tectonically exhumed ultra-high pressure rocks (see e.g. Chopin, 2003). The plume head is assumed to be

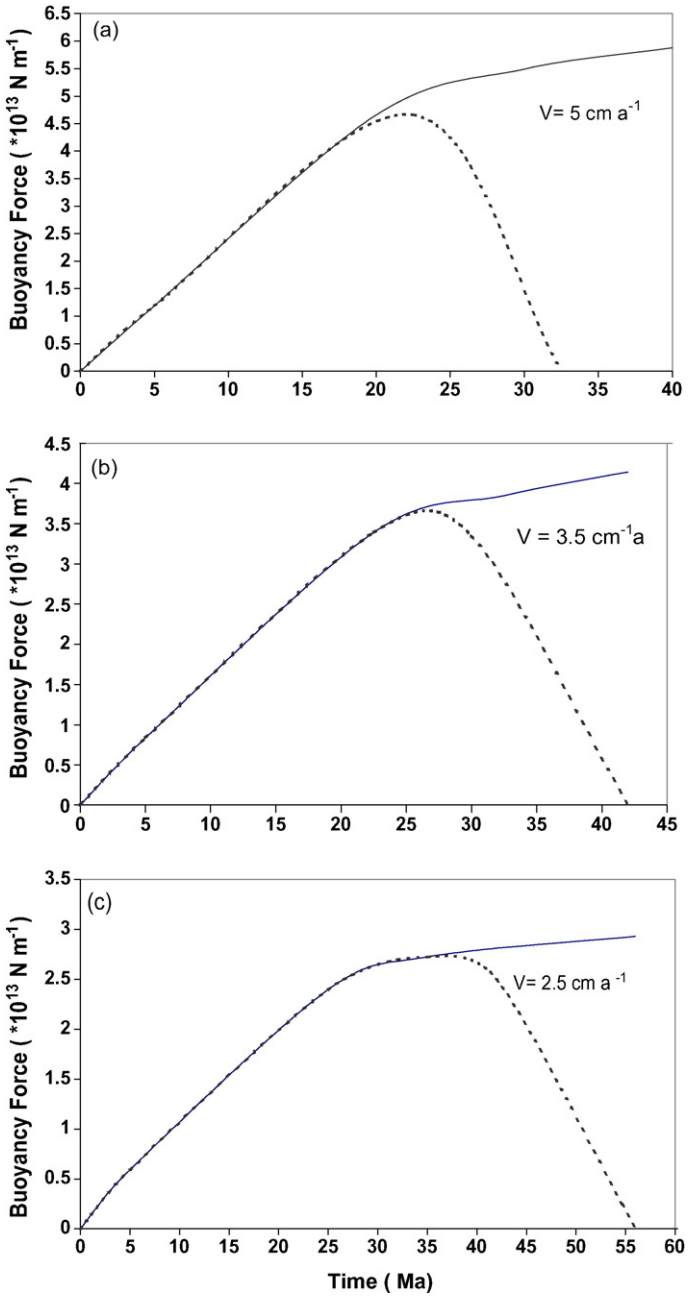

Fig. 4. Time evolution of negative buoyancy since the initiation of subduction for three constant suduction rates (a–c). The full line shows the negative buoyancy of a completely oceanic slab; the dotted line shows the negative buoyancy of an initially oceanic slab in which continental material begins to be subducted when the tip of the slab has reached the bottom of the mantle transition zone. See text for details.

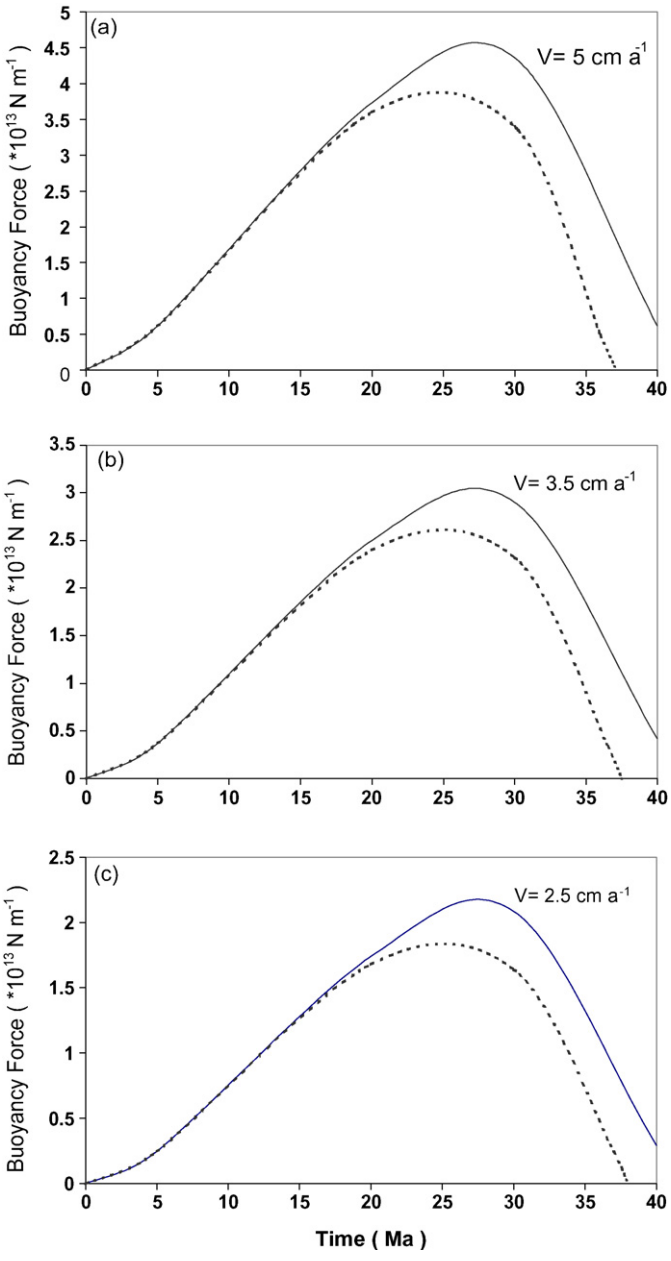

Fig. 5. Time evolution of negative buoyancy for three time-dependent subduction rates with different peak values (a–c). Rates increase exponentially during the first 5 Ma, stay constant at the peak value for the next 15 Ma, then decrease exponentially during the following 12 Ma. Full and dotted lines as in Fig. 4. Continental material begins to be subducted when the subduction rate begins to decrease (20 Ma).

in contact with the lower boundary of the slab between points P_1 and P_2, that is, in the 140–280 km depth range. Plume heads could be both wider and narrower than this, according to whether one deals with a full plume or with a more localized mantle diapir. However, the width of the plume is not an important factor in the present first-order model, as the total strength of the slab is estimated along 1-D profiles across the slab above the plume head.

The temperature distribution within the slab at the beginning of slab–plume interaction is obtained from the thermal models of Mahatsente and Ranalli (2004) and Ranalli et al. (2005). The plume head is assumed to be at $T = 1900$ K, that is, approximately 300 K hotter than the surrounding mantle. No relative motion is assumed to occur between slab and plume head, i.e., interaction begins when the subduction rate has become negligible. The plume head modifies the thermal evolution of the slab above it and decreases its strength. In order to model the thermal effect of the plume, the heat transfer equation is solved with the finite-difference code SHEMAT (Clauser, 2003). Values of the

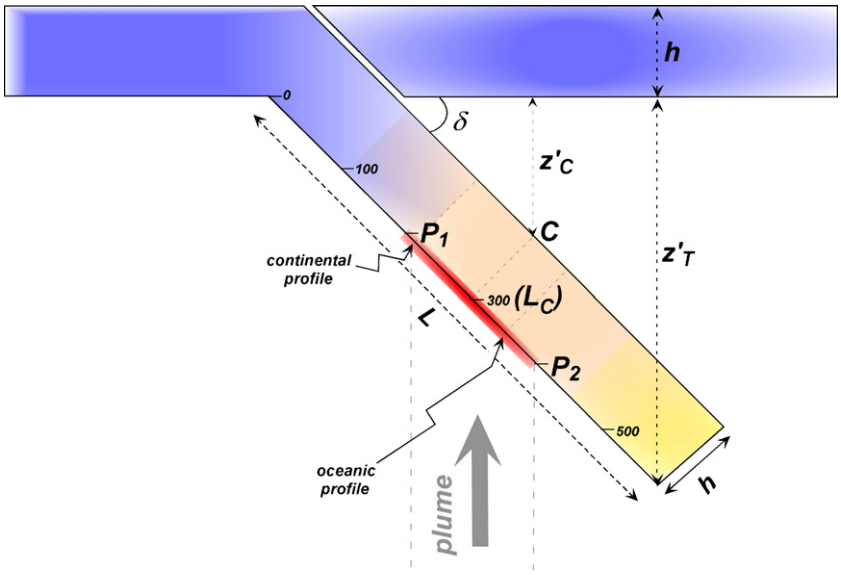

Fig. 6. Geometry of thermorheological model of oceanic-continental slab in contact with a plume head. See text for details.

parameters used in the thermal and rheological calculations are shown in Table 3. The chosen values are in the range usually adopted in geodynamic modelling (cf. e.g. Ranalli, 1995). The choice of constant thermal conductivity and capacity for each layer (continental crust, oceanic crust, and lithospheric mantle) introduces an error which is negligible in comparison with other uncertainties related to model assumptions and rheological parameters (the latter are discussed in the next paragraph). Two cases have been chosen as representative of relatively "cold" and "hot" subduction, the terms denoting the initial temperature distribution within the slab at the time of arrival of the plume. In the first case, the plume arrives 28 Ma after the initiation of subduction, when the slab is still relatively cold; in the second case, 37 Ma after the initiation of subduction, when the slab has had more time to equilibrate with the surrounding mantle. While the results of the model are purely indicative, these two cases have been chosen as possibly bracketing a range of real situations. The time-dependent temperature distribution within the slab for the first 20 Ma after the beginning of slab–plume interaction is shown in Fig. 7. The effect of the plume is considerably larger in the "cold" case, where the temperature within the slab above the centre of the plume is reduced by up to ∼300 K in 10 Ma. The effect would be correspondingly larger if slab–plume interaction occurred at shallower depth.

The strength of the slab above the plume is a function of its thermal state, and is estimated separately for its oceanic and continental parts (see Fig. 6 for location of profiles), as a function of time after initial contact with the plume. In the calculations, the oceanic part of the slab is assumed to consist of a 7 km thick crust (modelled with the rheology of dolerite), the continental part of a 30 km thick crust (modelled with the rheology of anorthosite), both overlying the lithospheric mantle for a total thickness of 100 km. The mantle is modelled with the rheology of dry peridotite, as deduced by a recent study of Gasperini et al. (2006) on ultramafic xenoliths from the Veneto Volcanic Province. Three rheological regimes are considered: (i) Coulomb frictional failure (Byerlee's law) which, however, is never predominant at the relevant temperatures; (ii) high-pressure failure (Shimada, 1993) with a strength of 200 MPa, which is predominant for the first few million years in the mantle part of the continental profile in the "cold" case; and (iii) non-linear viscosity (power-law creep; strain rate 10^{-14} s^{-1}) which is always predominant except where high-pressure failure applies. At any given point within the slab, the predominant mechanism is the one resulting in the lowest strength. We first estimate rheological profiles (strength envelopes; cf. Ranalli, 1995, for details) in the oceanic and continental parts of the slab above the plume head at different times since the arrival of the plume, then we obtain the total strength by integration of rheological profiles across the thickness of the slab.

The evolution of total strength along continental and oceanic profiles overlying the plume head for both "cold" and "hot" slabs is shown in Fig. 8 as a function of time since the arrival of the plume. The decrease in total strength is the combined

Table 3
Thermal and rheological parameters used in the modelling of slab–plume interaction (results shown in Figs. 7 and 8)

Material	K (W m^{-1} K^{-1})	C (MJ m^{-3} K^{-1})	A (MPa^{-n} s^{-1})	n	E (kJ mol^{-1})
Continental crust	2.5	2.24	3.3×10^{-4}	3.2	238
Oceanic crust	2.5	2.24	2.0×10^{-4}	3.4	260
Mantle	3.0	2.64	2.5×10^{4}	3.5	532

Symbols: K, thermal conductivity; C thermal capacity; A pre-exponential creep parameter; n stress exponent; E creep activation energy (the last three refer to the power-law creep equation).

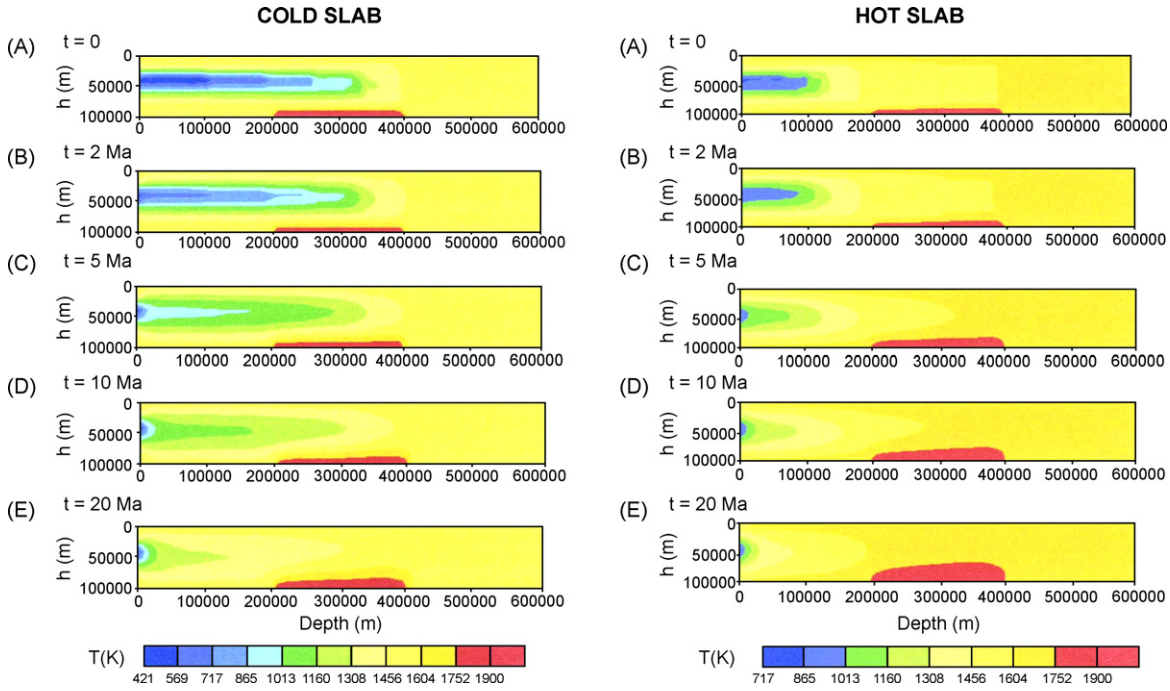

Fig. 7. Thermal evolution of a slab (with geometry as in Fig. 6) as a function of time since contact with the plume material. The vertical coordinate is the thickness of the slab; the horizontal coordinate is its downdip length measured along its lower boundary (both in metres). See text for discussion of conditions in the "cold" and "hot" case.

effect of thermal equilibration of the slab relative to the surrounding mantle and heat diffusion from the plume head. The relative importance of these two components is discussed in Section 6.2. In the "cold" case, the total strength of the continental part is higher than that of the oceanic part for approximately the first 10 Ma. This (and the shape of the curve) is due to the fact that the lithospheric mantle underlying the continental crust is relatively cold and consequently in the high-pressure failure regime. The continental total strength decreases by one order of magnitude in about 10 Ma, and afterwards becomes less than the oceanic total strength. In the "hot" case, both continental and oceanic strengths are more than one order of magnitude lower, and the continental strength is always lower than the oceanic strength. The significance of these results will be discussed in the following section.

6. Considerations on timing and depth of slab detachment

6.1. Effects of changes in negative buoyancy

Thermomechanical models of slab detachment (cf. e.g. Wong et al., 1997; Van de Zeedde and Wortel, 2001; Gerya et al., 2004) show that the timing and depth of detachment can vary greatly according to the controlling parameters. Van de Zeedde and Wortel (2001), for instance, predict mid-lithospheric detachment depths. On the other hand, Gerya et al. (2004) predict that detachment of an oceanic slab can occur ~10 Ma after the cessation of subduction if the slab is thin (~50 km), but requires times ≥30 Ma for slabs with thickness >80 km. The depth of detachment varies between ~100 and 250 km. Consequently, influx of deep material can occur within 10–30 Ma from the cessation of subduction.

The subduction of continental crust causes a decrease in negative buoyancy which generates tensional forces within the slab near the continent/ocean transition (Davies and von Blankenburg, 1995). These forces may lead to early slab breakoff. However, at least in cases where geological evidence shows that subducted continental material has been subject to ultra-high pressure (UHP) metamorphism, breakoff cannot have occurred in the very early stages of continental subduction (see Chopin, 2003, for a review of UHP metamorphism of continental crust).

For constant subduction rates, the negative buoyancy begins decreasing significantly within a few million years after the arrival of the leading edge of continental crust at the trench, and is reduced to about half its peak value in ~10–15 Ma (see Fig. 4). This range does not change significantly in the case of time-dependent subduction rate (Fig. 5), which shows that the main factor affecting total buoyancy is the positive buoyancy of continental material. Therefore, assuming that the likelihood of slab breakoff (other conditions being equal) is higher for larger negative buoyancies, the most favorable time interval for breakoff, for subduction velocities of a few cm a^{-1}, is within 10–15 Ma after the arrival of continental material at the trench. Detachment should occur, as proposed by Davies and von Blankenburg (1995) near the leading edge of continental material.

6.2. Effects of an impinging plume on slab strength

The time evolution of negative buoyancy alone does not allow more accurate predictions, since the actual time and depth of

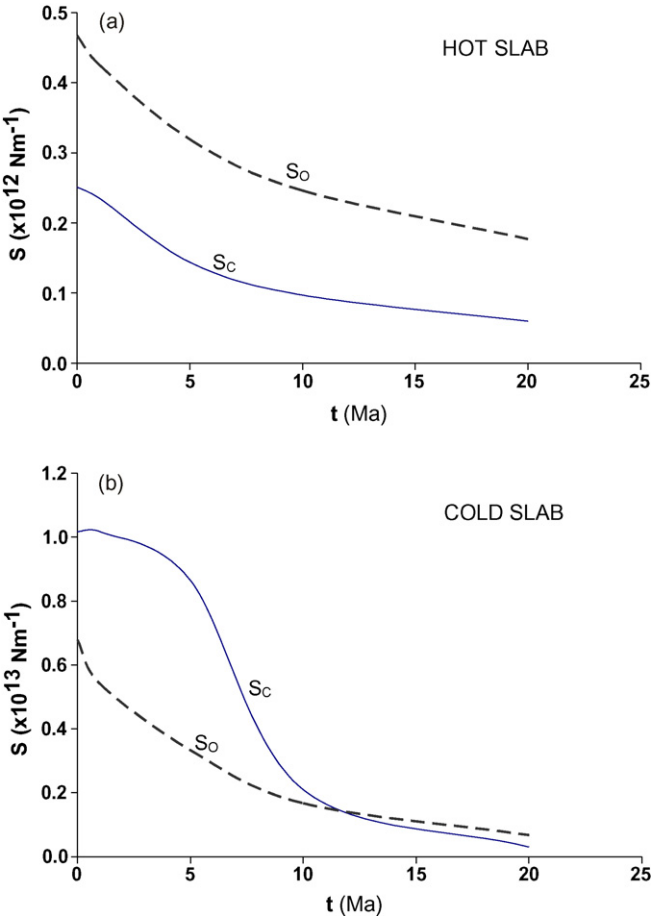

Fig. 8. Variation of the total strength of a "cold" and a "hot" slab above the plume head as a function of time elapsed since contact with the plume. The strength of the continental part is denoted by S_c (full line); that of the oceanic part by S_o (dashed line). See Fig. 6 for location of continental and oceanic profiles.

breakoff for a given slab depend on a balance between integrated stresses acting on the slab and total strength. The former is affected not only by buoyancy, but also by dynamic interactions between the slab and surrounding mantle; the latter is a function of temperature and the rheology of the slab. Assuming that detachment has not yet occurred, the plume head modifies the thermal evolution of the slab above it (see Fig. 7) and decreases its strength. The resulting rheological profiles across the slab, taken near the continent/ocean transition, result in the total slab strengths shown in Fig. 8 as functions of time since the arrival of the plume.

The decrease in slab strength caused by thermal diffusion from the plume head in the first 10 Ma amounts to ∼40–60% for "hot" slabs, and 60–80% for "cold" slabs (see Fig. 8; note, however, that the initial strength is one order of magnitude lower in the former case). This can be compared with the decrease in total strength of a stationary slab not interacting with a plume. Using the same procedure to compute temperature and strength, we find that in the case of a "hot" slab, the total strengths of the oceanic and continental profiles above the plume 10 Ma since plume arrival are reduced to approximately 2/3 and 1/2 of the values they would have in the absence of a plume, respectively. The corresponding values in the case of a "cold" slab are 1/2 and 1/3, respectively. Furthermore, the magnitude of the decrease for the "cold" case is larger, due to the higher initial values of total strength. Plume-induced heating is therefore a significant process.

Although a "hot" slab has total strength about one order of magnitude less than a "cold" slab (Fig. 8), its negative buoyancy is correspondingly less (Fig. 5). After ∼10 Ma since the arrival of the plume, the total strength of the slab has decreased considerably (almost one order of magnitude under "cold" conditions) and relatively stabilized. If plume-induced slab detachment is favored by a combination of significantly reduced total strength and still significant negative buoyancy, it is likely to occur in relatively cold slabs within a time window approximately 10–15 Ma after the arrival of the plume. The actual timing depends on several other factors (subduction rate, slab thickness, subduction dip angle, depth of slab–plume interaction), which however should not significantly change the above estimate.

In the cold case, the continental side of the slab is stronger than the oceanic side for approximately the first 10 Ma after the arrival of the plume. This fact and the rapid decrease of continental strength are a consequence of the relatively low temperatures of the continental mantle part of the slab, and the consequent high-pressure failure rheological regime. After 10 Ma, continental and oceanic strengths are not significantly different. Consequently, under typical "cold" conditions (fast subduction rates, short residence times), slab breakoff – if it does not occur on the oceanic side within the first 10 Ma – will probably occur at a position depending on the location of the plume. Under "hot" conditions (slow subduction velocities, long residence times), on the other hand, the continental side of the slab is always weaker than the oceanic side. In this case detachment, if mechanically feasible, should occur on the continental side.

7. Proposed petrogenetic model

In the light of geochemical and geophysical results we propose the following scenario (Fig. 9), which may serve as a working hypothesis for further more detailed work:

- During Paleocene time (∼60 Ma) the HIMU-OIB magmatism of the SEAV was able to manifest itself, as the upflow from the mantle encountered no obstacle.
- About 10 Ma later, the magmatic activity was stopped by the arrival of the lithospheric slab which trapped the ascending plume material.
- After approximately a further 10 Ma, (i.e. ∼45–40 Ma) the slab reached the conditions for its detachment.
- After detachment and opening of a plate window, mantle plume upwelling gave rise to the HIMU-DMM volcanism. Some of the plume material above the subducting slab provided further heating of the overriding mantle wedge to the point of promoting partial melting. The basic calc-alkaline magmas mixed with the HIMU-DMM component as suggested by isotopic data.

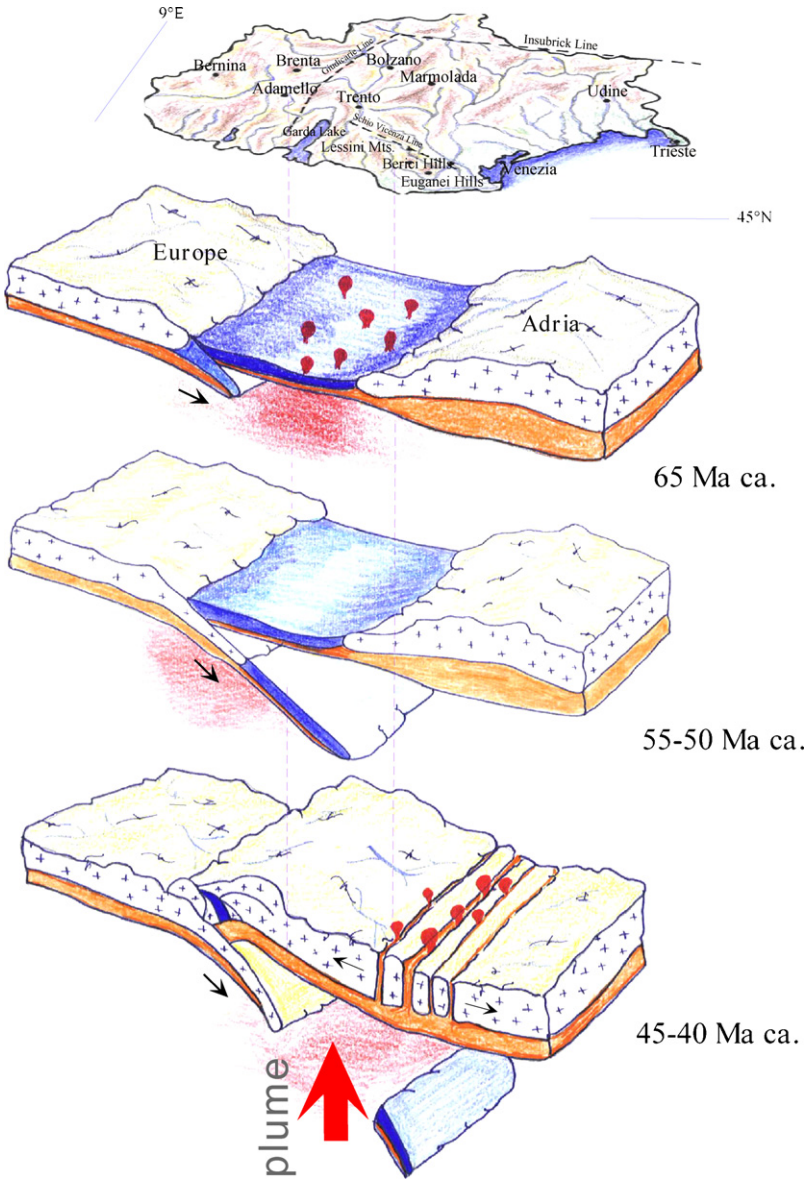

Fig. 9. Scenario for slab–plume interaction in Alpine belt evolution and magma genesis in the tertiary. Mantle plume upwelling is likely active since the Paleocene (about 65 Ma ago) and is represented as a red area/arrow below the lithospheric plate(s) in each portrait.

- Underplating by these basic magmas at the mantle–crust interface favoured partial melting of the lower crust with production of the TTG felsic suite of the Periadriatic Lineament. In this context it is important to note that the peak of alkaline magmatism in the Perialpine area (SEAV, ca. 45 Ma ago) preceded by only a few million years the calc-alkaline Periadriatic magmatism (ca. 42 Ma, age of Adamello gabbros).

8. Conclusions

Plume-related volcanism in subduction zones is possible either before the subducted slab intercepts mantle plumes, or after slab breakoff. Detachment is favoured by relatively fast subduction rates, subduction of continental material, and mantle plume upwelling. Negative buoyancy reaches its peak value within about 10 Ma after the decrease in subducion rate and/or the arrival of continental material at the trench, depending on subduction rate and history. If the slab comes into contact with a plume head, its total strength is reduced significantly in comparison to simple thermal relaxation. Under typical "cold" conditions (fast subduction velocities, short residence times), the total strength of the slab is reduced by almost one order of magnitude in about 10 Ma.

The above considerations provide a framework for the occurrence of plume-related and calc-alkaline magmatism in the southeastern Alps and probably in other similar tectonic settings, such as the Central Europe Magmatic Province. Upwelling of mantle diapirs through a plate window generated by slab detachment provide a petrogenetic model for the presence of mantle plume material in convergent settings which is compatible with geochemical evidence and first-order geodynamic modeling.

Acknowledgements

The work of P.M. and D.G. has been supported by Ministero Italiano Università Ricerca (MIUR) grant 2001048833 to P.M. G.R.'s research is supported by a grant from Natural Sciences and Engineering Research Council of Canada (NSERC); these funds also made possible R.M.'s stay at Carleton University as a Postdoctoral Fellow. We thank numerous colleagues who have read a preliminary version of this paper, and Advisory Editor Wolf Jacoby for advice during preparation of the final version.

References

Albarède, F., Gasperini, D., Blichert-Toft, J., Bosch, D., Del Moro, A., Macera, P., 2000. OIB-type magmas in subduction zones: mantle counterflow above detaching plates. EOS 81, 1271.

Aldanmaz, E., Pearce, J.A., Thirwall, M.F., Mitchell, J.G., 2000. Petrogenetic evolution of late Cenozoic, post-collision volcanism in western Anatolia, Turkey. J. Volcanol. Geother. Res. 102, 67–95.

Alibert, C., Michard, A., Albarède, F., 1983. The transition from alkali basalts to kimberlites: isotope and trace element evidence from melilitites. Contrib. Mineral. Petrol. 82, 176–186.

Alvarez, W., 1976. A former continuation of the Alps. Bull. Geol. Soc. Am. 87, 891–896.

Amodio-Morelli, L., et al., 1976. L'arco calabro-peloritano nell'orogene Appenninico-Maghrebide. Mem. Soc. Geol. Ital. 17, 1–60.

Barth, S., Oberli, F., Meier, M., 1989. U–Th–Pb systematics of morphologically characterized zircon and allanite; a high resolution isotopic study of the Alpine Rensen pluton (northern Italy). Earth Planet. Sci. Lett. 95, 235–254.

Beccaluva, L., Coltorti, M., Milani, L., Salvini, L., Siena, F., Tassinari, R., 2000. Tertiary nephelinite to tholeiite magma generation in the Veneto Volcanic Province. In: Southern Alps, Goldschmidt Conference, Oxford, England, 3–8 September.

Bellieni, G., Cavazzini, G., Fioretti, A.M., Peccerillo, A., Poli, G., 1991. Geochemical and isotopic evidence for crystal fractionation, AFC and crustal anatexis in the genesis of the Rensen Plutonic Complex (Eastern Alps, Italy). Contrib. Mineral. Petrol. 92, 21–43.

Bellieni, G., Cavazzini, G., Fioretti, A.M., Peccerillo, A., Zantedeschi, P., 1996. The Cima di Vila (Zinsnock) Intrusion, Eastern Alps: evidence for crustal melting, acid-mafic magma mingling and wall-rock fluid effects. Mineral. Petrol. 56, 125–146.

Bonardi, G., De Vivo, B., Giunta, G., Lima, A., Perrone, V., Zappetta, A., 1982. Mineralizzazioni dell'arco calabro-peloritano. Ipotesi genetiche e quadro evolutivo. Boll. Soc. Geol. Ital. 103, 279–309.

Bonin, B., 2004. Do coeval mafic and felsic magmas in post-collisional to within-plate regimes necessarly imply two contrasting, mantle and crustal, sources? A review. Lithos 78, 1–24.

Borsi, S., Del Moro, A., Sassi, F.P., Zipoli, G., 1979. On the age of the Vedrette di Ries (Rieserferner) massif and its geodynamic significance. Geol. Rundschau 68, 41–60.

Caggianelli, A., Del Moro, A., Paglionico, A., Piccarreta, G., Pinarelli, L., Rottura, A., 1991. Lower crustal granite genesis connected with chemical fractionation in the continental crust of Calabria (Southern Italy). Eur. J. Mineral. 3, 159–180.

Castellarin, A., Piccoli, G., 1966. I vulcani eocenici dei dintorni di Rovereto. Giornale di Geologia 33 (2), 291–365.

Cebria, J.M., Lopez-Ruiz, J., 1995. Alkali basalts and leucitites in an extensional intracontinental plate setting: the late Cenozoic Calatrava Volcanic Province (Central Spain). Lithos 35, 27–46.

Cebria, J.M., Lopez-Ruiz, J., Doblas, M., Oyarzun, R., Hertogen, J., Benito, R., 2000. Geochemistry of the quaternary alkali basalts of Garrotxa (NE Volcanic Province, Spain): a case of double enrichment of the mantle lithosphere. J. Volcanol. Geotherm. Res. 102, 217–235.

Chopin, C., 1984. Coesite and pure pyrope in high-grade bluenshists of the western Alps: a first record and some consequences. Contrib. Mineral. Petrol. 86, 107–118.

Chopin, C., 2003. Ultrahigh pressure metamorphism: tracing continental crust into the mantle. Earth Planet. Sci. Lett. 212, 1–14.

Clauser, C. (Ed.), 2003. Numerical Simulation of Reactive Flow in Hot Aquifers. Springer, Berlin.

Clocchiatti, R., Del Moro, A., Gioncada, A., Joron, J.L., Mosbah, M., Pinarelli, L., Sbrana, A., 1994. Assessment of a shallow magmatic system; the 1888–1890 eruption Volcano Island, Italy. Bull. Volcanol. 56, 466–486.

Coulon, C., Megartsi, M., Fourcade, S., Maury, R.C., Bellon, Louni-Hacini, A., Cotton, J., Coutelle, A., Hermitte, D., 2002. Post-collisional transition from calc-alkaline to alcaline volcanism during the Neogene in Oranie (Algeria): magmatic expression of a slab breakoff. Lithos 62, 87–110.

Dal Piaz, G.V., Venturelli, G., Scolari, A., 1979. Calc-alkaline to ultrapotassic post-collisional volcanic activity in the Internal Northwestern Alps. Mem. Soc. Geol. Padova 32, 4–16.

Dal Piaz, G.V., Venturelli, G., 1983. Brevi riflessioni sul magmatismo post-ofiolitico nel quadro dell'evoluzione spazio-temporale delle Alpi. Mem. Soc. Geol. Ital. 26, 5–19.

Dal Piaz, G.V., Del Moro, A., Martin, S., Venturelli, G., 1988. Post-collisional magmatism in the Ortler-Cevedale massif (Northern Italy). Jb. Geol. B. A. 131, 533–551.

Dal Piaz, G.V., Gosso, G., 1994. Some remarks on evolution of the Alpine lithosphere. Quaderni di Geodinamica Alpina e Quaternaria 2, 93–101.

Dal Piaz, G.V., Cortiana, G., Del Moro, A., Martin, S., Pennacchioni, G., Tartarotti, P., 2001. Tertiary age and paleostructural inferences of the eclogitic imprint in the Austroalpine outliers and Zermatt-Saas ophiolite, western Alps. Int. J. Earth Sci. (Geol. Rundsch) 90, 668–684.

Dal Piaz, G.V., Bistacchi, A., Massironi, M., 2003. Geological outline of the Alps. Episodes 26 (3), 175–181.

Dalrymple, G.B., Clague, A.C., Tracy, L.V., 1987. 40Ar/39Ar age, petrology, and tectonic significance of some seamounts in the Gulf of Alaska. In: Keating, B.H., Fryer, P., Batiza, R., Boehlert, G.W. (Eds.), Seamounts, Islands, and Atolls, American Geophysics Union Monograph, vol. 43. AGU, Washington, DC, pp. 297–315.

Davies, J.H., von Blankenburg, F., 1995. Slab breakoff: a model of lithosphere detachment and its test in the magmatism and deformation of collisional orogens. Earth Planet. Sci. Lett. 129, 85–102.

Davis, A.S., Clague, D.A., Gray, L.B., Hein, J.R., 2002. The Line Islands revised: new 40Ar/39Ar geochronologic evidence for episodes of volcanism due to lithospheric extension. Geochem. Geophys. Geosyst. 3, doi:10.1029/2001GC000190.

Del Moro, A., Pardini, G., Quercioli, C., Villa, I.M., Callegari, E., 1983. Rb/Sr and K/Ar chronology of the Adamello granitoids, Southern Alps. Mem. Soc. Geol. Ital. 26, 285–301.

Del Moro, A., Paglionico, A., Piccarreta, G., Rottura, A., 1986. Tectonic structure and post-Hercynian evolution of the Serre, Calabrian arc, Southern Italy: geological, petrological and radiometric evidence. Tectonophysics 124, 223–238.

Dercourt, J.F., et al., 1986. Geological evolution of the Tethys from the Atlantic to the Pamirs since the Lias. Tectonophysics 123, 241–315.

Deutsch, A., 1984. Young Alpine dikes south of the Tauern Window (Austria): a K–Ar and Sr isotopic study. Contrib. Mineral. Petrol. 85, 45–57.

De Vecchi, G., Sedea, R., 1974. Sui basalti Eocenici dei Colli Euganei. Mem. Inst. Geol. Miner. Univ. Padova 31, 25.

De Vecchi, G., Sedea, R., 1995. The Paleogene basalts of the Veneto Region (NE Italy). Mem. Sci. Geol. 47, 253–274.

Dobosi, G., Fodor, R.V., Goldberg, S.A., 1995. Late-Cenozoic alkalic basalt magmatism in northern Hungary and Slovakia: petrology, source compositions and relationship to tectonics. Acta Vulcanol. 7 (2), 199–207.

Docherty, C., Banda, E., 1995. Evidence for the eastward migration of the Alboran sea based on regional subsidence analyses: a case for basin formation by delamination of the subcrustal lithosphere? Tectonics 14, 804–818.

Downes, H., Pantò, G., Poka, T., Mattey, D.P., Greenwood, P.B., 1995a. Calc-alkaline volcanics of the inner Carpathian arc, Northern Hungary: new geochemical and oxygen isotopic results. Acta Vulcanol. 7 (2), 29–41.

Downes, H., Vaselli, O., Seghedi, I., Ingram, G., Rex, D., Coradossi, N., Pecskay, Z., Pinarelli, L., 1995b. Geochemistry of late Cretaceous-early Tertiary magmatism in Poiana Rusca (Romania). Acta Vulcanol. 7 (2), 209–217.

Duggen, S., Hoernle, K., Van den Bogaard, P., Garbe-Schönberg, D., 2005. Post-collisional transition from subduction—to intraplate-type magmatism in the westernmost Mediterranean: evidence for continental-edge delamination of subcontinental lithosphere. J. Petrol. 46 (6), 1155–1201.

El Bakkali, S., Gourgaud, A., Bourdier, J.L., Bellon, H., Gundogdu, N., 1998. Post-collision neogene volcanism of the Eastern Rift (Morocco): magmatic evolution through time. Lithos 45, 523–543.

Faccenna, C., Mattei, M., Funiciello, R., Jolivet, L., 1997. Styles of back-arc extension in the central Mediterranean. Terra Nova 9, 126–130.

Franzini, M., Leoni, L., Saitta, M., 1975. Revisione di una metodologia analitica per fluorescenza-X, basata sulla correzione completa degli effetti di matrice. Rend. Soc. Ital. Miner. Petrol. 31, 365–378.

Frey, M., Desmons, J., Neubauer, F. (Eds.), 1999. The new metamorphic map of the Alps: Schwez. Mineral. Petrogr. Mitt. 79, 1–230.

Gasperini, D., Blichert-Toft, J., Bosch, D., Del Moro, A., Macera, P., Albarède, F., 2002. Upwelling of deep mantle material through a plate window: evidence from the geochemistry of Italian basaltic volcanics. J. Geophys Res. 107 (B12), 2367, doi:10.1029/2001JB000418.

Gasperini, D., Maffei, K., Piromallo, C., Macera, P., Faccenna, C., Martin, S., Ranalli, G., 2003. Where is the tail of the European plume volcanism? In: EGS-AGU-EUG Joint Assembly, Nice, France, 6–11 April.

Gasperini, D., Bosch, D., Braga, R., Bondi, M., Macera, P., Morten, L., 2006. Petrology and Sr–Nd–Pb–O isotope composition of mantle xenoliths from the Veneto Volcanic Province (North-eastern Italy). Geochem. J. 40 (4), 377–404.

Gerya, T.V., Yuen, D.A., Maresch, W.V., 2004. Thermomechanical modelling of slab detachment. Earth Planet. Sci. Lett. 226, 101–116.

Goes, S., Spakman, W., Bijwaard, H., 1999. A lower mantle source for central European volcanism. Science 286, 1928–1931.

Granet, M., Wilson, M., Achauer, U., 1995. Imaging a mantle plume beneath the Massif Central (France). Earth Planet. Sci. Lett. 136, 281–296.

Hansmann, W., Oberli, F., Steiger, R.H., 1983. U–Pb ages on zircon from the Southern Adamello. Mem. Soc. Geol. Ital. 26, 319–321.

Harangi, S., 2001. Neogene to quaternary volcanism of the Carpathian-Pannonian Region—a review. Acta Geologica Hungarica 44 (2–3), 223–258.

Harangi, S., Tonarini, S., Vaselli, O., Manetti, P., 2003. Geochemistry and petrogenesis of Early Cretaceous alkaline igneous rocks in Central Europe: implications for a long-lived EAR-type mantle component beneath Europe. Acta Geologica Hungarica 46, 77–94.

Harangi, S., 2004. Origin of the common enriched mantle component in the Neogene volcanic rocks of the Mediterranean and the Carpathian-Pannonian region. In: 32nd International Geological Congress, Florence, Italy, 20–28 August.

Hickey, R.L., Frey, F.A., Gerlach, D.C., Lopez-Escobar, L., 1986. Multiple sources for basaltic arc rocks from the southern volcanic zone of the Andes (34°–41° S): trace element and isotopic evidence for contribution from subducted oceanic crust, mantle and continental crust. J. Geophys. Res. 91 (B6), 5963–5983.

Hoernle, K., Zhang, Y.S., Graham, D., 1995. Seismic and geochemical evidence for large-scale mantle upwelling beneath the eastern Atlantic and western and central Europe. Nature 374, 34–39.

Jung, S., Hoernes, S., 2000. The major-and trace-element and isotope (Sr, Nd, O) geochemistry of Cenozoic alkaline rift-type volcanic rocks from the Rhon area (Central Germany): petrology, mantle source characteristics and implications for asthenosphere–lithosphere interactions. J. Volcanol. Geotherm. Res. 99, 27–53.

Juteau, M., Michard, A., Albarède, F., 1986. The Pb–Sr–Nd isotope geochemistry of some recent circum-mediterranean granites. Contrib. Mineral. Petrol. 92, 331–340.

Langmuir, H., Vocke, R.D., Hanson, G.N., Hart, S.R., 1978. A general mixing equation with application to Icelandic basalts. Earth Planet. Sci. Lett. 37, 380–392.

Leoni, L., Saitta, M., 1976. X-ray fluorescence analysis of 29 trace elements in rock and mineral standards. Rend. Soc. Ital. Mineral. Petrol. 32, 497–510.

Luciani, V., 1989. Stratigrafia sequenziale del Terziario nella catena del Monte Baldo (Provincie di Verona e Trento). Mem. Sci. Geol. XLI, 263–351.

Keskin, M., 2003. Magma generation by slab steepening and breakoff beneath a subduction-accretion complex: an alternative model for collision-related volcanism in Eastern Anatolia, Turkey. Geophys. Res. Lett. 30, doi:10.1029/2003GL018019, 24.8046.

Macera, P., Ferrara, G., Pescia, A., Callegari, E., 1983. A geochemical study on the acid and basic rocks of the Adamello batholith. Mem. Soc. Geol. Ital. 26, 223–259.

Macera, P., Del Moro, A., Martin, S., Pieroni, M., Tambellini, K., 1998. The role of the lower crust on the genesis of mafic and felsic rocks from the Adamello batholith (Southern Alps); geochemical and isotope (Sr–Nd) evidence. Mem. Soc. Geol. Ital. 50, 74–77.

Macera, P., Gasperini, D., Piromallo, C., Blichert-Toft, J., Bosch, D., Del Moro, A., Martin, S., 2003a. Geodynamic implications of deep mantle upwelling in the source of Tertiary volcanics from the Veneto region (South-Eastern Alps). J. Geodyn. 36, 563–590.

Macera, P., Gasperini, D., Maffei, K., Martin, S., Piromallo, C., 2003b. Tertiary magmatism in the eastern Alps. Mem. Sci. Geol. 54, 119–122.

Macera, P., Gasperini, D., Piromallo, C., Funiciello, F., Faccenna, C., Ranalli, G., 2004. Recent hot spot volcanism in the European and Mediterranean area. In: 32nd International Geological Congress, Florence, Italy, 20–28 August.

Mahatsente, R., Ranalli, G., 2004. Time evolution of negative buoyancy of an oceanic slab subducting with varying velocity. J. Geodyn. 38, 117–129.

Malamud, B.D., Turcotte, D.L., 1999. How many plumes are there? Earth Planet. Sci. Lett. 174, 113–124.

Marchant, R.H., Stampfli, G.M., 1997. Subduction of continental crust in the Western Alps. Tectonophysics 269, 217–235.

Milani, L., Beccaluva, L., Coltorti, M., 1999. Petrogenesis and evolution of the Euganean magmatic complex, Veneto Region, North-East Italy. Eur. J. Mineral. 11, 379–399.

Peccerillo, A., 2003. Plio-Quaternary magmatism in Italy. Episodes 26, 222–226.

Peccerillo, A., 2005. Plio-Quaternary Magmatism in Italy. Spinger, Berlin.

Piromallo, C., Faccenna, C., 2004. How deep can we find the traces of Alpine subduction? Geophys. Res. Lett. 31, doi:10.1029/2003GL019288.

Ranalli, G., 1995. Rheology of the Earth, second ed. Chapman & Hall, London.

Ranalli, G., Pellegrini, R., D'Offizi, S., 2000. Time dependence of negative buoyancy and the subduction of continental lithosphere. J. Geodyn. 30, 539–555.

Ranalli, G., Gasperini, D., Macera, P., Mahatsente, R., 2004. Subduction of continental lithosphere, changes in negative buoyancy, and slab–plume interaction: consequences for slab breakoff. In: EGU General Assembly, Nice, France, 25–30 April.

Ranalli, G., Martin, S., Mahatsente, R., 2005. Continental subduction and exhumation: an example from the Ulten Unit, Tonale Nappe, Eastern Austroalpine. In: Gapais, D., Brun, J.P., Cobbold, P.R. (Eds.), Deformation Mechanisms, Rheology and Tectonics: From Minerals to the Lithosphere. Geol. Soc. London, pp. 159–174 (Special Publication).

Ritter, J.R.R., Jordan, M., Christensen, U.R., Achauer, U., 2001. A mantle plume below the Eifel volcanic fields, Germany. Earth Planet. Sci. Lett. 186, 7–14.

Rosembaum, J.M., Wilson, M., Downes, H., 1997. Multiple enrichment of the Carpathian-Pannonian mantle: Pb–Sr–Nd isotope and trace element constraints. J. Geophys. Res. 102, 14947–14961.

Schmid, S.M., Pfiffner, O.A., Schonborn, G., Froitzheim, N., Kissling, E., 1997. Integrated cross section and tectonic evolution of the Alps along the eastern traverse. In: Pfiffner, O.A., Lehner, P., Heitzman, P., Mueller, S., Steck, A. (Eds.), Results of NPR 20, Deep structure of the Swiss Alps. Birkhaeuser Verlag Publishers, Basel, Switzerland, pp. 289–304.

Shimada, M., 1993. Lithosphere strength inferred from fracture strength of rocks at high confining pressures and temperatures. Tectonophysics 217, 55–64.

Stampfli, G.M., Mosar, J., Favre, P., Pillevuit, A., Vannay, J.C., 2001. Permo-Mesozoic evolution of the western Tethyan realm: the Neotethys/East-Mediterranean connection. In: Ziegler, P.A., Cavazza, W., Robertson, A.H.F. (Eds.). PeriTethys memoir 6: Peritethyan rift/wrench basins and passive margins, vol. 186, Crasquin-Soleau, S., IGCP 369, pp. 51–108, Mém. Museum Nat. Hist. Nat.

Szabo, C., Harangi, S., Csontos, L., 1992. Review of Neogene and quaternary volcanism of the Carpathian-Pannonian region. Tectonophysics 208, 243–256.

Thorpe, R.S., Francis, P.W., O'Callaghan, L., 1984. Relative roles of source composition, fractional crystallization in the petrogenesis of Andean volcanic rocks. Philos. Trans. R. Soc. London (Ser A) 310, 675–692.

Van de Zeedde, D.M., Wortel, M.J.R., 2001. Shallow slab detachment as a transient source of heat at midlithospheric depths. Tectonics 20, 868–882.

Vaselli, O., Downes, H., Thirlwall, M., Dobosi, G., Coradossi, N., Seghedi, I., Szakacs, A., Vannucci, R., 1995. Ultramafic xenoliths in Plio-Pleistocene alkali basalts from the Eastern Transylvanian Basin: depleted mantle enriched by vein metasomatism. J. Petrol. 36, 23–53.

Venturelli, G., Thorpe, R.S., Dal Piaz, G.V., Del Moro, A., Potts, P.J., 1984. Petrogenesis of calc-alkaline shoshonitic and associated ultrapotassic Oligocene volcanic rocks from the Northwestern Alps, Italy. Contrib. Mineral. Petrol. 86, 209–220.

von Blankenburg, F., Davies, J.H., 1995. Slab breakoff: a model for syncollisional magmatism and tectonics in the Alps. Tectonics 14, 120–131.

Wilson, M., Downes, H., 1991. Tertiary–quaternary extension-related alkaline magmatism in western and central Europe. J. Petrol. 32, 811–849.

Wilson, M., Bianchini, G., 1999. Tertiary–quaternary magmatism within the Mediterranean and surrounding regions. In: Durand, Jolivet, Horvath, Seranne (Eds.). The Mediterranean Basins: Tertiary extension within the Alpine orogen, vol. 156, pp 141–168. Geol. Soc. London, Special publication.

Wilson, M., Patterson, R., 2002. Intraplate magmatism related to short-wavelenght convective instabilities in the upper mantle: evidence from the tertiary–quaternary volcanic province of western and central Europe. Geological Society of America, vol. 352, pp. 37–58 (special papers).

Wong, A., Ton, S.Y.M., Wortel, M.J.R., 1997. Slab detachment in continental collision zones: an anlysis of controlling parameters. Geophys. Res. Lett. 24, 2095–2098.

Ziegler, P.A., 1992. European Cenozoic rift system. In: Ziegler, P.A. (Ed.), Geodynamics of Rifting, vol. 1, Tectonophysics, 208, 91–111.